To,
Dr. N.V. Joshi

FORECASTING SPATIALLY STRUCTURED POPULATIONS: IMPLICATIONS FOR RESOURCE EXPLOITATION

Mark S. Boyce*

Madhav Gadgil

N. V. Joshi

V. Nanjundiah

Center for Ecological Sciences

and

Center for Theoretical Studies

Indian Institute of Science

Bangalore 560 012

INDIA

RUNNING HEAD: SPATIAL POPULATION FORECASTING

*Current address: Department of Zoology & Physiology, University of Wyoming, Laramie, WY 82071-3166 USA.

$$X_1' = (1-D) r X_1(1-X_1) + D r X_2(1-X_2)$$
$$X_2' = D r X_1(1-X_1) + (1-D) r X_2(1-X_2)$$

Summed:

$$X' = r X_1(1-X_1) + r X_2(1-X_2)$$
$$= r(X - X1{*}{*}2 - X2{*}{*}2).$$

ABSTRACT

We study the deterministic dynamics of 2 difference equation models for spatially structured populations, differing in the manner in which dispersal occurs among subpopulations. These models afford a broad spectrum of dynamics, including intermittency where populations move in and out of chaos to either periodic fluctuations or equilibrium. Low to intermediate levels of dispersal usually have a dampening effect on population fluctuations driving populations from chaotic fluctuations to periodicity or equilibrium. For high dispersal rates, we observe rapid convergence in the dynamics of subpopulations so that the entire metapopulations behaves as a single population.

Ability to forecast future populations tends to deteriorate with increasing dispersal up to a threshold above which high dispersal rates cause convergence in dynamics of subpopulations. Nonlinear forecasting is perfect when the dynamics are periodic. Asynchrony of subpopulations makes it impossible to accurately forecast the dynamics of the metapopulation as a whole although forecasting may be highly successful for individual subpopulations. Forecasting methods are not highly effective for populations exhibiting intermittency in dynamics between chaos and periodicity or equilibrium. Because spatial structure can destroy the characteristic projection interval signature for chaos, nonlinear forecasting cannot be employed as a reliable tool for detecting chaos from noise in spatially structured populations.

Forecasting population behavior is of obvious value in resource exploitation and conservation. In general, we suggest that forecasting at local scales holds promise, and may indeed help us to understand highly developed resource-exploitation strategies employed by local indigenous humans. Our observations suggest that attempts to apply resource exploitation strategies at regional scales may yield poor results.

KEYWORDS: CHAOS, DENSITY DEPENDENCE, DISPERSAL, FISHERIES, FORECASTING, METAPOPULATIONS, NONLINEAR DYNAMICS, RESOURCE MANAGEMENT, TIME SERIES, TRIBALS

1. INTRODUCTION

Spatial structure can substantially complicate population dynamics, especially when individual subpopulations are unstable (May 1989, Hassell et al. 1991). Yet, we believe that such complexity is a widespread, if not universal, phenomenon in natural populations. In this paper we study the dynamics of simple models of spatially structured populations, with an emphasis on developing an understanding of how these dynamics evolve. We then consider how spatial structure affects the utility of nonlinear forecasting both for detecting nonlinear structure in the constituent subpopulations (Sugihara and May 1990), and for applications in resource exploitation.

1.1 Assumptions

The structure of the models which we explore is based upon some basic assumptions about population dynamics for species which are typically exploited by humans, e.g., plants in the forest, fisheries, wildlife. We focus our attention to tropical regions where we believe that it is most likely that biological interactions and thereby nonlinear dynamics will have the greatest effect on the dynamics of populations and communities. We believe this to be true because in general the intensity biological interactions appears to be greater in the tropics (Dobzhansky 1950), and as the connectedness and complexity of biological communities increases, they are less likely to be stable (May

1975). We also note May's (1987) contention that exploited populations are amongst those most likely to exhibit chaotic dynamics. Indeed, many populations in tropical regions certainly show substantial fluctuations (Wolda 1975, Gadagkar & Sundarara 1985) despite the expectation that unpredictable climatic rigors have less bearing on populations in the tropics than in more temperate regions (MacArthur 1972).

Although we recognize that there is still debate about the relevance of chaos in biological populations, there is no question that nonlinear structure is fundamental to any model of ecological interactions. We will not attempt to review the biological and statistical evidence for chaos in ecological systems (see Sugihara and May 1990, Logan and Main 1992), although we note that sufficiently long time series necessary to make a satisfactory evaluation are scarce. Rather we will stand behind the clear understanding that biological interactions are inherently nonlinear, and the systems we consider are among the most likely to be unstable and thereby show complex dynamics (May 1986, 1987; Schaffer 1985, 1988).

1.2 Relation to metapopulations

Levins (1969, 1970) coined the terminology of metapopulation for populations that are spatially structured into numerous subpopulations. And he went on to show how the interaction between extinction and colonization can help us to understand the dynamics and distribution of a species' occupancy of subpopulations.

Indeed, most investigations of metapopulation dynamics have focussed upon the role of extinction and colonization in spatially-structured populations (Gilpin and Hanski 1991). Hanski and Gilpin (1991) claim that "the key processes in metapopulation dynamics are extinction and colonization."

Yet, it is not always the case that the dynamics of regional populations are governed largely by the processes of extinction and colonization (Harrison 1991). Dispersal alone can be an important process structuring the dynamics of regional or metapopulations.

We do not wish to encourage semantic debate regarding the definition of metapopulation, but wish to make it clear that extinction and recolonization are not processes we have studied. Rather we envision model species that are relatively abundant, disperse among subpopulations, and are not subject to local extinctions. As a frame of reference we have been thinking about coastal marine fisheries, and plant and animal populations exploited by tribals in forests of India. But we believe these models have much broader applicability.

1.3 Modes of Dispersal

As May (1989) and Hassel et al. (1991) have suggested, the manner in which dispersal occurs among subpopulations is likely to affect the dynamics that emerge from the system. Hassell et al. assumed rates of dispersal which were density independent, although dispersal was proportional to population size. Even though rates of dispersal are not strictly density dependent, because more animals leave high-density areas and fewer leave low-density areas, the net effect is density dependent. This effect can be made even stronger by defining the rate of dispersal to be a direct function of dispersal. Either form of dispersal has the potential to stabilize the dynamics of populations because emigration may be high when densities become large and/or immigration from surrounding populations may bolster population size when it is small.

We expect that density-dependent rates of dispersal will occur as an adaptive response by individuals to local density conditions, whereas an innate propensity for dispersal amongst individuals in a population may be density independent. The distinctions and consequences for the evolution of dispersal are developed by Gadgil (1971) and Comins et al. (1980).

Spatial scales, modes of locomotion, spatial heterogeneity, and behavior can all influence the manner in which organisms disperse into surrounding areas. Dispersal rates may vary as a function of age or phenotype (Lomnicki 1988), or may be a complex function of distance among sites. To limit the scope of our analysis, we will consider only 2 modes of dispersal: (1) dispersal occurs only amongst n adjacent cells or subpopulations during each time interval, and (2) a dispersal pool of floaters develop that may ~~are equally likely to~~ settle in any of n subpopulations.

1.4 Organization of this paper

Our objective is to understand the role of dispersal in population dynamics and forecasting, so we will begin by limiting spatial structure to simple 2-celled populations and then expand the analysis to more complex spatial configurations. Finally we discuss the ramifications for the exploitation and conservation of natural resources.

2. MODELS

To achieve an understanding of the complexities imposed by spatial structure in fluctuating populations we have explored the behavior of simple models with very simple spatial structure. In all examples the underlying dynamics derive from a difference equation approximation of the logistic model extracted from the fisheries literature (Ricker 1954):

$$F(X) = X * \exp[r(1 - X/K)] \qquad \text{(eq. 2.1)}$$

which we use to iterate the dynamics of X individuals governed by a potential growth rate r, defining the carrying capacity, K, to be the positive critical point. Dynamics of this model have been studied extensively, and can be summarized by the familiar Hopf bifurcation diagram in Figure 2.1.

Use of this difference equation is justified on the grounds that such a discrete-time model can capture the essential behavior of more complex models (Schaffer 1985). Specifically, we assume that this model may approximate a 1-dimensional map of a multi-species system in continuous time. And certainly it is the case that the spectrum of dynamical behaviors emanating from this model can be found in nature (Logan and Main 1992, Turchin and Taylor 1992).

We have studied the dynamics of 2 mathematical models, each with dispersal among subpopulations. Except where specified otherwise, we assume a homogeneous environment with r_i's and K_i's equivalent among subpopulations. We considered models where (1) dispersal is simply proportional to population size, and (2) dispersal is a quadratic function of density. As spatial structure increases, the complexity of interactions increases. Therefore, we will first consider the models where only 2 interacting subpopulations exist.

2.1 Proportional dispersal

In our first model, dispersal occurs proportional to population size, and it happens subsequent to recruitment within each subpopulation. For subpopulations i and j, we define an innate rate of dispersal, δ, and dispersal mortality, μ, subscripted i,j for movement from subpopulation i to subpopulation j. For simplicity we will combine these terms into a realized dispersal rate $D_{ij} \equiv \delta_{ij}(1 - \mu_{ij})$. Following the structure of Gadgil's (1971) first model we write

$$X_i' = (1 - D_{ij})F_i(X_i) + D_{ji}F_j(X_j) \qquad \text{(eq. 2.2)}$$

Here the net effect of dispersal may involve either emigration or immigration depending upon whether population i is smaller or larger than subpopulation j respectively.

To generalize to more complex spatial patterns, we calculate interactions between n subpopulations pairwise subsequent to population growth and $D_j \equiv D_{ij} = D_{ji}$. This yields

$$X_i' = F(X_i) + \sum_{j=1}^{n} D_j[F_j(X_j) - F_i(X_i)] \qquad \text{(eq. 2.3)}$$

constrained for $D_j < 1/n$ and $i \neq j$.

2.2 Density-Dependent Dispersal

In our second model the rate of emigration from a subpopulation depends upon population size in a quadratic fashion, but otherwise the model is like eq. 2.2:

$$X_i' = F_i(X_i) - [F_i(X_i)]^2 D_{ij} + [F_j(X_j)]^2 D_{ji} \qquad \text{(eq. 2.4)}$$

and more generally

$$X_i' = F_i(X_i) - [F_i(X_i)]^2 D_{ij} + \sum_{j=1}^{n} [F_j(X_j)]^2 D_{ji} \qquad \text{(eq. 2.5)}$$

where again, we set constraints for $D < 1/n$ and $i \neq j$.

$-x^2 \qquad (Q-x)^2$

$r\{x - x^2 + y - y^2$

$-Q^2 + 2Qx - x^2$

$Q' = r\{$

$r[Q - Q^2 + 2x(Q-x)]$

$2x(Q-x)$

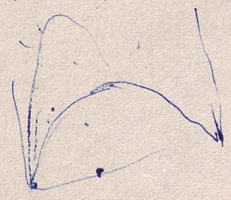

10 Nov 92

$$x' = Ax(1-x) + By(1-y)$$
$$y' = Bx(1-x) + Ay(1-y)$$

Equil $\cancel{Ax^2}$ $(A-1)x - Ax^2 + By - By^2 = 0$

$\cancel{Bx}$ $- Bx^2 + (A-1)y - Ay^2 = 0$

$x' = \lambda x(1-x)$ $1 - 1/\lambda$

$\delta x' = \lambda - 2\lambda x$

$\lambda(1-2x)$

$-\lambda(1-2x) \cdot \lambda\left(1 - 2\frac{(\lambda-1)}{\lambda}\right)$

$\lambda - 2\lambda + 2 = 2-\lambda$

$\lambda = 3$

$$-B(A-1)x + BAx^2 - B^2y + B^2y^2 = 0$$
$$+ABx - ABx^2 + A(A-1)y - A^2y^2 = 0$$

$$x + (A^2 - 1 - B^2)y = (A^2 - B^2)y^2 = 0$$

$A = (1-D)\lambda$

$B = D\lambda$

$D = 0$ check $\lambda = 2$

$D = 1/2$

$D = 1/4$

$\lambda \ne B = 1$

$B = 1/2$ $A = 3/2$

D	1/4	1/2	3/4	
A	2	3/2	1	1/4
B	0	1/2	1	3/4

$\lambda = 2$

use ~~D for D = 1/2~~

$1/2\, x - \frac{3}{2}x^2 + 1/2\, y - 1/2\, y^2 = 0$

$1/2\, x - 1/2\, x^2 + 1/2\, y - 3/2\, y^2 = 0$

Eq.

$1/2\, x$

$-1/4 + By - By^2$

$-(B - 1/2)^2$

λ

$\sqrt{A} \pm \sqrt{Z} = -\frac{(A-1)^2}{4A}$

$R \mp P x^2 \mp Q y^2 = 0$

$\sqrt{A}x - Q$

$-Ax^2 + 2\sqrt{A}Q - Q^2$

$= A - 1$

$Z = \frac{A-1}{2\sqrt{A}}$

$-(\sqrt{B}y - Z)^2$

$-By^2 + 2\sqrt{B}yZ - Z^2$

$-\cancel{By}\ -By^2$

$2\sqrt{B}yZ = B\cancel{y}$

$Z = \frac{\sqrt{B}}{2}$ $Z^2 = \frac{B}{4}$

$x = 0, y = 1$

$+\frac{B}{4} - \left(\sqrt{B}y - \frac{\sqrt{B}}{2}\right)^2$

$+\frac{B}{4} - B\left(y - 1/2\right)^2$

$+ \frac{(A-1)^2}{4A} - \left(\sqrt{A}x - \frac{A-1}{2\sqrt{A}}\right)^2 = 0$

$-(\sqrt{A}x \mp Z)^2$

$-Ax^2 + 2\ldots$ $+Z^2$

$2\sqrt{A}Z - Z^2$

$= (A-1)$

$\frac{(A-1)^2}{4A}$

$Z = \frac{A-1}{2\sqrt{A}}$

$+ 1/4 + \frac{(A-1)^2}{4A} - (y - 1/2)^2 - ($

$Mx^2 + Ny^2 = L$

3. DYNAMICS OF 2-CELLED MODELS

3.1 Proportional Dispersal

The dynamics of this model span the entire range of dynamics described by May (1976), plus some patterns which we have not seen before. For readers not familiar with the dynamics of the basic Ricker model, we recommend the paper by May and Oster (1976) as background for the following.

We find that the behavior of these models can be better understood heuristically by examining piecewise one-dimensional maps of the components, and we have used this approach variously throughout the next section.

3.1.1 Effect of dispersal

With no dispersal, D = 0, each population behaves independently. If initial population sizes are different, even by a small amount, chaotic dynamics diverge and there is no correlation between future populations. Each population is governed by its own 1-dimensional map, but because the 2 populations are not synchronous, the summed total population (ΣX) is not so well behaved. This is illustrated in Figure 3.1.1a where we first show a 1-D map for subpopulation i governed by $r_i = 3.5$, securely in the chaotic region, with a Lyapunov exponent of -x.x. Mapping $X_j(t+1)$ against $X_i(t)$ shows what is essentially randomness between the 2 subpopulations (Fig. 3.1.1b). Yet, because the

$Q' = x(Q - Q^2$

$x^2 2Qx - 2x^2$

$2x(Q-x)$

$Ax \, B(1-x) + B(Q-x)(1-Q-x$

$x' + y' = (A+B)(x(1-x) + (A+B)y(1-y)$

$(A+B)(x(1-x) + y(1-y)$

$= x + y - x^2 - y^2$

$y = Q - x$

$y^2 = Q^2 + 2Qx - x^2$

underlying 1-D map for X_i carries half of the dynamics for the total population, there is clearly structure in the 1-D map for the summed total population (Fig. 3.1.1c).

For positive values of D increasing up to D = 0.021, the effect of dispersal dampens population fluctuations as reflected by reduced coefficient of variation in population size (Fig. 3.1.2) and a progressively decreasing Lyapunov exponent (Fig. 3.1.3). Dynamics in this range can be characterized by those appearing at D = 0.02 illustrated at Figure 3.1.4. The basic population behavior can be again characterized by the underlying 1-D map for equation 2.1 illustrated at Figure 3.1.4a. For proportional dispersal, after recruitment, a constant proportion of X_i is subtracted to represent the i-subpopulation animals emigrating (Fig. 3.1.4b), and then supplemented by some fraction of X_j coming in from subpopulation j. The manner in which emigration occurs in the model essentially scales down the map at Figure 3.1.4a, yielding a map (Fig. 3.1.4c) that invariably has a smaller Lyapunov exponent and therefore greater stability (i.e., reference here is to the intermediate map, still independent of X_j).

On the otherhand, subpopulation j has the potential to be totally independent of i. Or it may be correlated by extrinsic perturbations (see Gilpin 1990). But here we assume independence except via dispersal, thus, attempting to map $X_j(t + 1)$ on $X_i(t)$ may not show much pattern (Fig. 3.1.4d). The next step in calculating $X_i(t + 1)$ is to sum the map in Fig. 3.1.4c with that in 3.1.4d, yielding the ultimate 1-D map for X_i (Fig. 3.1.4e). Because of the strength of the underlying map for X_i, and the low extent of dispersal (note we multiply D = 0.02 times the scale on Fig. 3.1.4d), the sum of Figures 3.1.4c and 3.1.4d still has its basic structure, but is made somewhat fuzzy by immigration, with negative displacements for large values near the peak of the map, and positive displacements for small values of $X_i(t+1)$ along the right-hand tail of the map.

For slightly higher dispersal, D = 0.0213, chaos begins to erode into quasi-periodic oscillations and eventually periodic behavior for D = 0.035. Bifurcations to periodicity occur in this region, e.g., at D = 0.0245 we find 18-point cycles (see Figure 3.1.5). For D = 0.03 we find smooth oscillations forming a striking set of maps (Figure 3.1.6). Ultimately, however, the entire dynamics collapse to a simple 2-cycle for each subpopulation and coincident equilibrium for the sum of the 2 subpopulations (Fig. 3.1.7) for $0.034 < D < 0.176$. Even in the domain of the 2-cycle, increasing D continues to have a stabilizing effect as reflected by decreasing $CV(X_i)$ as shown back in Figure 3.1.2.

Abruptly at D = 0.177, the map of ΣX begins to take structure again (Fig. 3.1.8a), and indeed look like an overgrown version of the 1-D map for X_i (Fig. 3.1.1a). Likewise, the X_i map restores much of its former shape, albeit a bit fuzzy (Fig. 3.1.8b). The map of net dispersal takes on a curious shape (Fig. 3.1.8c), and the phase plot begins to appear squeezed into a cigar shape (Fig. 3.1.8d). What is emerging is that the dynamics for the 2 subpopulations are converging as a consequence of high D. Intermittency is a common feature of time series for D values in this range, with populations bouncing in and out of quasi-periodic oscillations and chaos (Fig. 3.1.8e).

By D = 0.21, the populations are approaching complete convergence--inspection of the time series of differences shows just the occasional burst of excitement (Fig. 3.1.9a), and the phase diagram is beginning to look like a fuzzy line (Fig. 3.1.9b). And at D = 0.22 the convergence is virtually complete after 200 iterations. At this point, the total population emerges chaotic with a simple 1-D map (Fig. 3.1.10), and constituent maps for X_i and X_j that are essentially identical to Figure 3.1.1a.

For dispersal coefficients between 0.22 and 0.8, the chaotic dynamics are consistently as expected from a single-population model. In most biological populations, we suspect that D is seldom larger than 0.5 since for D > 0.5 we observe inverse density dependence. That is, subpopulations with relatively high density get even more dispersers. Yet, perhaps such aggregation phenomena are more common than our intuition would suggest (Kareiva and Odell 1986).

In the vicinity of D = 0.8, synchrony between X_i and X_j begins to break down as reflected by bursts of dispersers appearing in the time series of dispersers (Figure 3.1.11). Then between D = 0.8 and D = 0.825 we witness the evolution of equilibrium populations for both X_i and X_j. In the next 2 sets of figures we will detail the emergence of these equilibria.

Note that the number of dispersers undergo fits of intense activity around values of -2 and 2.36 when D = 0.82 as illustrated in Figure 3.1.12a. These are reflected by intermittency in the time series for X_i and X_j with critical points apparent at 0.5 and

2.38 (Fig. 3.1.12b). These emerging critical points are readily identified on the 1-D map for X_i shown in Figure 3.1.12, panel c. At this D value, the map for X_i is virtually identical to that of X_j. But for slightly larger values of D, the map locks into one critical point or the other--in the case of the X_i map plotted in Figure 3.1.12f, activity converges on $X_i = 0.5$. And eventually this becomes a stable point. It is rather arbitrary which subpopulation (i or j) converges on 0.5 vs. 2.4, and the outcome is solely determined by the initial values. Changing the initial value for X_i to a value larger than X_j results in equilibrium of 2.4 for X_i and 0.5 for X_j.

For the total population, the outcome for each individual population is arbitrary, with a clear stable equilibrium emerging on the 1-D map (Fig. 3.1.13) with convergence occurring at $\Sigma X = 2.88$. We have numerically estimated the eigenvalue associated with this critical point, $\lambda = -1.x$, which is clearly stable.

Equilibrium is maintained for D increasing up to 0.967, above which we go through yet another final phase of intermittency with periodic and quasi-periodic oscillations, and increased variation in both X's and the ΣX. The final map for $X_j(t+1)$ on $X_i(t)$ when D = 1 is identical to the map of X_i for D = 0, as indeed it should be (recall Fig. 3.1.1a). When D = 1, dispersal entails the entire population from cell i switching places with the entire population from cell j. Thus, the maps for ΣX are likewise identical for D = 0 and D = 1 (see Fig. 3.1.1c-h).

The dynamics as a function of D are summarized in a bifurcation diagram plotted at Figure 3.1.14, and an overview of the dynamics emerging from this model is provided in Table 1.

3.1.2 Spatial Heterogeneity

The above calculations all assume equal r's and K's as would be observed in a homogeneous environment. Of course, much of spatial variation can be attributed to spatial variation in habitat (Wildlife 2000, ref?) which would have the effect of altering r's and K's. We have studied the proportional dispersal model by systematically varying r_i's and K_i's, and generally find that dispersal has an averaging effect.

Remarkably complex dynamics can appear when both populations have r's are in the chaotic range, but as the disparity in r's becomes greater, it becomes more likely that simple periodic or equilibrium dynamics will dominate.

Patterns are perhaps best summarized by referencing the CV plots and bifurcation diagrams for 3 new combinations of r's. In Figure 3.1.15 we summarize the results of simulations where r_i = 3.5 and r_j = 2.7 (the latter value being near the chaotic threshold for individual populations), and the corresponding bifurcation plot in Figure 3.1.16. As in the homogeneous environment example detailed above...

Similar things appear when r_i = 3.5 and r_j = 2.0 (Figs. 3.1.17 and 3.1.18) although here... Finally, we show an extreme case where r_i = 3.5 and r_j = 1.0 (Figs. 3.1.19 & 3.1.20). Here the dynamics are periodic throughout, with 3-cycles appearing for small

D, and 2-cycles for larger values of D. In each of these examples, when D > 0.5, the fluctuations are greater for subpopulation j than for i simply because more of i's population is moving into cell j than are remaining in i.

Disparity between K's has complicating consequences as well. Periodicity can appear for even small values of D, and the dynamics of the system become dominated by the larger of the 2 populations. This is understandable since for proportional dispersal there will usually be a net dispersal from the more abundant population. Since the respective K determines the average population sizes, dispersal will tend to be from the population with the higher K to that with the lower K.

Sample bifurcation diagrams and associated CV plots are presented in Figure 3.1.21 and 3.1.22. Note that for very small values of D, with $K_i = 1.0$ and $K_j = 2.0$ (see Fig. caption for other particulars), we incur a 3-cycle, but only for a narrow band of D values. That this should occur can be appreciated by inspecting the bifurcation diagram for the independent Ricker function (Fig. 2.1) and noting a small region of 3-cycles appearing near r = 3.2. We interpret our 3-cycle as a consequence of dispersal pushing the 1-D map just far enough to gain the symmetry necessary for a 3-cycle. In ecological systems, it seems highly unlikely that such fine structure could ever be observed for very long since a small amount of variance in r (or virtually any parameter) will push the dynamics into the broader regions of chaos.

3.2 Density-Dependent Dispersal

Density dependence has the effect of dampening population fluctuations, and structurally we find similar results here as for proportional dispersal. Because the dispersal terms are squared, to place D's on the same scale as for proportional dispersal, we plot results as a function of the square root of D. In Fig. 3.2.1 we present the plot of CV's for this model, which mirror those found for the proportional dispersal. As D increases, variation decreases as the populations go through a phase of quasi-periodic behavior. In the midst of this there is a brief span of D values over which a 6-cycle is supported; this breaks down and ultimately collapses to a simple 2-cycle for each subpopulation and equilibrium for the total population.

Before the 2-cycle breaks down, here we see the total population develop a 2-cycle as well. Then the 2 subpopulations converge so that the total population takes on a clean 1-D map reflecting the dynamics for the synchronous population as a whole.

Before $D^{0.5}$ reaches 0.5, however, severe overshoots begin to develop and some interesting nonlinearities emerge in the maps. The phase map develops a peculiar bulge (Fig. 3.2.2) and the 1-D map for X_i takes on a precarious shape in Figure 3.2.3 with a few values approaching 4. These overshoots indeed become so violent that calculation is not possible for $D^{0.5}$ much greater than 0.5 because negative populations appear.

In Figure 3.2.4 we present the bifurcation diagram for this model. Different nonlinear shapes appear in the maps for model 2.4

than for model 2.2, but for the most part, the dynamics are quite similar between the 2 models.

4. ALTERNATIVE SPATIAL CONFIGURATIONS

4.1 Dispersal Pool Models

As modelled by Gadgil (1971), we can envision dispersal involving the formation of a dispersal pool of individuals ready to colonize sites when they become available. Such a dispersal pool of "floaters" appears to exist in many avian populations (ref.).

To simulate such a dispersal pool, we used a 9-cell model as at equation 2.3 where each of the 9 cells enjoyed equal dispersal rate exchanges with each of the other 8 cells. To avoid new individuals to be "created" by dispersal, the maximum D we will entertain is 0.125. All cells were assigned equivalent r_i's at 3.5, and K's were assumed to be 1.0. Initial X_i's were arbitrarily assigned to cell 1, 2, ..., 9 values equal to 0.1, 0.2, ..., 0.9.

In comparison with the complex array of dynamics which we observed for the 2-cell model, the dynamics here are relatively straight forward. The plot of CVs shows that for exceptionally low D values we lock into periodic behavior. Then we go through a transition towards convergent dynamics and for D > xx, the entire system behaves as a single chaotic population.

Periodic behavior and convergence emerge at low values of D because of the strong averaging effect imposed by the dispersal pool.

4.2 Linear-chain Models

Again we use a 9-cell model, but instead of dispersal occurring among all cells, it only happens between adjacent cells in a linear chain of cells. Therefore, n will be 2 at most, and only 1 for the cells occurring at the ends of the chain. Sample calculations are based upon equation 2.3 with equal r's and K's. All cells were assigned equivalent r_i's at 3.5, and K's were assumed to be 1.0. Initial X_i's were arbitrarily assigned to cell 1, 2, ..., 9 values equal to 0.1, 0.2, ..., 0.9.

Our motivation behind this spatial organization came from an interest in the marine fisheries along the west coast of India where fish populations are distributed essentially in a linear fashion. Similarly, such organization is a reasonable way to consider populations of aquatic organisms occupying a stream or river where dispersal occurs between adjacent subpopulations.

We resort to the CV plot to provide an overview of the dynamics of this system (Fig. 4.2). Qualitative patterns can be drawn from the simpler 2-cell model, except...

4.3 Grid Models

Again, this is a variation on equation 2.3 but where the cells are arranged in a 3x3 grid. In such a configuration, cells on the corner interact with 2 adjacent cells. Cells located in the middle on each of the 4 sides have 3 other cells with which they interact, and the central cell exchanges dispersers with each of these 4 cells. All cells were assigned equivalent r_i's at 3.5, and K's were assumed to be 1.0. Initial X_i's were arbitrarily assigned to cell 1, 2, ..., 9 values equal to 0.1, 0.2, ..., 0.9.

Because of there exist 3 distinct types of cells depending upon the assignment on the grid, there are more complex dynamics that appear in the previous models we have studied. Again, an overview can be had from a plot of CV's presented in Figure 4.3. Even though each cell is identical in all regards except the number of dispersing interactions, the dynamics can be quite different from cell to cell. For example, it is not uncommon to have equilibrium appearing in one cell whilst adjacent cells may be undergoing chaotic oscillations. ...

5. BOUNDARY PROBLEMS

The models which we have discussed thus far all assume reflecting boundaries, i.e., when dispersing individuals encounter a boundary which is not contiguous with another subpopulation, individuals will not disperse. Such an assumption is valid for species that do not venture into habitats incapable of supporting the species.

Yet such an assumption is species dependent, and the extreme alternative assumption is that non-contiguous boundaries are absorbing, and that dispersers are simply lost to the population.

These boundary considerations are highly dependent not only on the behavior of the species in question, but also on the specific geometry of the habitat. examples...SPOW? Rvw Lande (1987)...

5.1 Circle-chain Models

One way to explore the consequences of reflecting boundaries in the above models is to eliminate the boundary. This is possible in 2-dimensions for the linear-chain model by connecting the ends to create a circle-chain. In Figure 5.1 we show the plot of $CV(X_5)$ and $CV(\Sigma X)$, and observe that ...

6. NONLINEAR FORECASTING

Spatial structure in populations complicates the ability to employ nonlinear forecasting techniques as proposed by Sugihara and May (1990). There are several approaches to nonlinear forecasting which have been reviewed by Casdagli (1989). In our discussions we have either employed a polynomial auto-regressive model ("global method"), or a local projection procedure using polynomial mappings in phase space as described by Sugihara and May (1990) and Schaffer and Tidd (1990).

6.1 Consequences of Dispersal

For each of the above models, when $D = 0$, and subpopulations are governed by r values in the chaotic range, the nonlinear forecasts follow a classic signature for a chaotic system as described by Sugihara and May (1990) for a range of ϵ values (see Figure 6.1.1). For model 2.2... At the opposite extreme, when $D = 1$, with a map as at Figure 3.1.1<u>b</u>, we see that the forecasting ability is much weaker (Fig. 6.1.2)

As D increases for small values above 0, forecasting ability into the future becomes progressively weaker until the system's dynamics become periodic (Fig. 6.1.3). As periodic behavior is approached, we see the tail of the forecast interval function lift until at truly periodic behavior the system is completely predictable for indefinite intervals into the future (Fig. 6.1.4). As D gets even larger and the system again leaves periodic behavior whilst converging upon synoptic chaos, we see the reemergence of the classic chaos forecasting signature (Figure 6.1.1).

6.2 Effect of r and K

In nature, of course, we see heterogeneity among sites which constitutes spatial variance in r and or K for the models considered here. Indeed, different sites are expected to be on different attractors which characterize the dynamics of the biotic community in a locality. It is of interest to see how well a forecasting model can be applied from one area to another where the system is on a different attractor.

We begin by examining predictions made by a global forecasting method. We estimated parameters for a 2-dimensional auto-regressive polynomial forecasting model using least squares (ref.). We then calculated the correlation between 1-year predictions based upon this model and "observed" values from a 2-cell proportional dispersal model (eq. 2.2) using various values of r. A summary of these calculations is presented in Figure 6.2.1. The r^2 values suggest that we can forecast remarkably well when r values are in regions of equilibrium, periodic or quasi-periodic fluctuations. This occurs even though the numerical predictions may be off substantially. For example, in a periodic population, a high value is likely to be followed by a low value--and the same is true when moving about on the chaotic map.

To better understand the accuracy of forecasts we calculated also the sums of squares of deviations between predicted and observed values as well as mean deviance [Σ(observed - predicted)]. Taking these together with r^2 we get a more complete picture of forecasting ability. In general, as one might expect, forecasts constructed from a time series based upon $r = 3.5$ are best for other time series with r values in the vicinity of 3.5 and generally deteriorate further away. Forecasting of populations in the periodic and quasi-periodic range generally yields quite high r^2 values even though accuracy may be poor.

Ability to forecast is also highly dependent upon knowledge of K. This can present some very real problems in nature because it can be very challenging to arrive at reliable estimates of population size (Seber 1982). Mean deviance between predicted and observed forecasts increases approximately exponentially for increasing or decreasing K (Figure 6.2.2). For example a 50% underestimate of K results in mean deviance which is 11.8 times that for forecasts where K is precisely determined. Likewise, overestimates by 50% result in xxx times the mean deviance.

6.3 Forecasting Periodicity

In deterministic simulations, local forecasting is perfect for periodic and quasi-periodic populations. This is true simply because it only requires a small number of mappings of future population to capture the systems dynamics in the local forecasting library. In nature, however, such periodicity is unlikely to be mapped so perfectly, being eroded by noise in various components of the system. The consequence of this noise to a periodically fluctuating system depends to some extent upon the behavior of the system for parameter values within some error region. If phase locking (Schaffer 1988) or other mechanism sustains periodicity of a particular frequency over a wide range of parameter values, perturbations will not push the system out of the periodic range, and forecasting predictions will have flat signatures which Sugihara and May (1990) would characterize as being simply noise. We show an example of this from our 2-celled model with $D = 0.1$ and other parameters as at Figure 3.1.2, where a 2-cycle is sustained for $0.034 < D < 0.176$, a span of $D = 0.142$. We have incorporated multiplicative noise with $\pm$ bounds of 0.15, 0.5, and 0.9. For low and intermediate levels of noise, forecasting ability does not decay with increasing forecast interval (Figure 6.3.1).

Yet, it is often the case that periodicity appears in a relatively small region of parameter space, e.g., note the 3-cycle toward the right-hand-side of the Ricker equation plot in Figure 2.1. When this happens, stochasticity has a propensity to launch the time series into forays of chaos. And the resulting forecast interval signatures are just like Sugihara and May (1990) characterized as being chaos with noise. To illustrate this we chose the familiar 2-cell case as before but here with D = 0.025 where X_i trains at an 18-cycle in the deterministic case. This periodicity is, however, only sustained over the interval of D = 0.0244-0.0252, a span of only D = 0.008. Here, although forecasting is perfect without noise, forecasting ability erodes with forecast interval even for relatively low inputs of multiplicative noise (Figure 6.3.2)

Chaotic systems frequently embrace parameter space in which periodicity appears--the Ricker map in Figure 2.1 offers several examples, most notably the region of a 3-cycle. Yet, if a deterministic system happens to be in one of these periodic tracks or a nearby quasi-periodic orbit, forecasting gives us no insight whatsoever into the intrinsic nonlinearity. But a little noise may be sufficient to make it appear.

6.4 Forecasting Intermittency

When structure exists in 1-D maps, one can usually do reasonably well at forecasting future populations. However, when intermittency in behavior occurs, i.e., with the time series moving in and out of chaos, forecasting models do quite poorly.

As an illustration, in Figure 6.4.1 we present a time series of X_i (panel <u>a</u>) and ΣX (panel <u>b</u>) for the 2-cell proportional dispersal model where with D = 0.178. Note periods of diverging oscillations towards chaos appearing around yrs 105 - 140 ~~xxx and xxx.~~ In Figure 6.4.2 we show the corresponding 1-D maps. Notice that the 1-D map actually has more structure than does the individual population. This structure passes into the forecast model as well, and in Figure 6.4.3 the effectiveness of local forecasting models is shown where the top curve represents the coefficients of determination for the map of the total population.

Intermittency is a very common phenomenon in these spatial models, particularly those with greater complexity in spatial structure. And as one might expect, the behavior is most common for values of D that cause transition from one type of dynamics into another, i.e., where we see transitions occurring between chaotic and periodic or equilibrium behavior.

6.5 Robustness of Forecasting Models

Explain how it is that a forecasting model constructed for a particular attractor can be superimposed upon another attractor and still yield high forecasting ability...

We note that r^2 often does a poor job of characterizing the deviations from an underlying model. If a model has any tendency toward periodic behavior, the apparent fit of the model will be greatly exaggerated due to ~~to~~ severe non-homogeneity of variances (see Sokal and Rohlf 198x). Indeed, the fit between predicted and observed can take some rather bizarre shapes as illustrated here in Figure 6.5.2. So some of the statistical robustness for forecasting models reflected in r^2 values may actually be an artifact of using an inappropriate statistical characterization.

The high forecasting ability for r = 2.8 offers an example. Here, note that the dynamics are essentially chaotic, but all motion is restricted to 2 bands of high and low X (see Figure 2.1). Successive iterations of equation 2.1 map back and forth across the gap which occurs between high and low values of X. When forecasting successive values of X we find that our accuracy is often not high within either the high or the low band of X's, but because these bands are separated, the r^2 of predictions appear quite high (see Figure 6.5.3).

6.6 Forecasting Metapopulations

In general, 1-dimensional maps for total populations are much less structured than for the constituent subpopulations (see §3.1), and therefore, one would expect lower forecasting capability for metapopulations than for subpopulations. To illustrate this we have calculated local forecasting models for each of 6 different chaotic 2-cell ΣX time series (Fig. 6.6.1) corresponding with the 1-D maps presented in Figure 3.1.1. In each case, as before, K_i = K_j = 1.0, D = 0, and $r_i = r_j$. These generally show, especially for short forecasting projections, poorer forecasting ability than in previously presented examples of subpopulation forecasting.

We then asked how well one might be able to forecast an independent subpopulation based upon a forecast model constructed from a metapopulation. [this bit was foiled--will resume later]

7. IMPLICATIONS FOR RESOURCE EXPLOITATION AND CONSERVATION

Forecasting of future population trajectories would have obvious value to fisheries and wildlife management in anticipating resource levels and developing optimal harvest policies.

7.1 Intermittency in Population Behavior

One of the intriguing types of dynamical behaviors common to these models in intermittency where populations will move in and out of chaos, periodicity, and equilibrium through time (Figure x). This would, of course, cause resource managers substantial difficulty if a pattern were observed, strategic management programs implemented, only to have these programs become superannuated upon the emergence of a new sort of dynamics. Indeed, forecasting models constructed ....

7.2 Forecasting Local versus Regional Populations

In general, one can realize much better success attempting to forecast local subpopulations than summed total populations in the 2 spatially structured models which we studied. This generalization holds true only for populations with limited dispersal ability, since extensive dispersal can result in the metapopulation behaving synchronously with subpopulations. A further limitation on the generalization is that difficult-to-forecast intermittency within subpopulations may be averaged out in the total population which may then be easier to forecast (recall §6.4).

For resource management agencies attempting to regulate resource exploitation, we would expect to find greatest success for such ventures when developed at a local level. Regulations applied at a regional, say state or provincial, level would be expected to be unsuccessful. Likewise, attempts to employ detailed harvest models (see Walters 1986) are likely to be highly unreliable if generalized over too large an area.

7.3 Tribal Localization

Motivation for this paper came largely from the observation by anthropologists that resource exploitation strategies are often quite specialized and localized by indigenous human groups, especially in tropical regions. For example, in India there are xxx recognized native tribes each occupying a specific locality and exploiting natural resources from a small geographic locality. Consistent with the predictions of our modelling results, it would make sense that localized specialization of resource exploitation strategies would develop which may not be very efficient over larger geographic areas (cite Gadgil and Berkes 1991)...

7.4 Forecasting in Conservation

The ability to forecast population trajectories might offer a method for "population viability analysis" (Soule 1987) to anticipate the probability of extinction. ARIMA forecasting methods have been used to project the population trajectory for the endangered Whooping Crane (<u>Grus americanus</u>) (Boyce and Miller 1985), and applications of forecasting in conservation have been reviewed by Dennis et al. (1991).

10. LITERATURE CITED

*Anderson, R. M., D. M. Gordon, M. J. Crawley, and M. P. Hassell. 1982. Variability in the abundance of animal and plant species. Nature 296:245-248.

Boyce, M. S., and R. S. Miller. 1985. Auk

Comins, H. N., W. D. Hamilton, and R. M. May. 1980. Evolutionary stable dispersal strategies. Journal of Theoretical Biology 82:205-230.

Dennis, B., et al. 1991. Ecol. Monogr.

Dobzhansky, T. 1950.

Gadagkar, S. R., and N. Sundararaj. 1985. Temporal behaviour of marine landings along coastal Karnataka. I. Relative distribution and secular trends. Fishery Technology 22:14-23.

Gadgil, M. 1971. Dispersal: Population consequences and evolution. Ecology 52:253-261.

Gadgil, M., and F. Berkes. 1991. Traditional resource management systems. Resource Management and Optimization 18:127-141.

Gilpin, M. 1990. Extinction of finite metapopulations in correlated environments. Pages 177-186 in B. Shorrocks and I. R. Swingland, eds. Living in a patchy environment. Oxford Univ. Press, Oxford, UK. 246pp.

Gilpin, M., and I. Hanski. 1991. Metapopulation dynamics: Empirical and theoretical investigations. Academic Press, New York.

*Hanski, I. 1987. Cross correlation in population dynamics and the slope of spatial variance-mean regressions. Oikos 50:149-

151.

Hanski, I., and M. Gilpin. 1991. Metapopulation dynamics: Brief history and conceptual domain. Biological Journal of the Linnean Society 42:3-16.

Harrison, S. 1991. Local extinction in a metapopulation context: An empirical evaluation. Biological Journal of the Linnean Society 42:73-88.

Hassell, M. P., R. M. May, and W. W. Pacala. in press. The persistence of host-parasitoid associations in patchy environments: I, a general criterion. Am. Nat. (in press)

Hassell, M. P., H. N. Comins, and R. M. May. 1991. Spatial structure and chaos in insect population dynamics. Nature 353:255-258.

Hutchinson, G. E.

Kareiva, P., and G. M. Odell. 1986. Swarms of predators exhibit 'preytaxis' if inidividual predators use area restricted search. Am. Nat. 130:233-270.

Levins, R. 1969. Some demographic consequences of environmental heterogeneity for biological control. Bull. Entomol. Soc. Amer. 15:237-240.

Levins, R. 1970. 1970. Extinction. Pages 75-108 in M. Gerstenhaber, ed. Some mathematical questions in biology. American Mathematical Society, Providence, Rhode Island, USA

Logan, J., and F. Main (eds.) 1992. Does chaos exist in ecological systems? University of Virginia Press (in press).

Lomnicki, A. 1988. Population biology of individuals... Princeton University Press, Princeton, NJ, USA.

MacArthur, R. H. 1972. Geographical ecology. Harper and Row, New York.

May, R. M. 1975. Stability and complexity in model ecosystems (2nd ed.). Princeton University Press, Princeton, NJ, USA.

May, R. M. 1976. Simple mathematical models with very complicated dynamics. Nature 261:459-467.

May, R. M. 1986. When two and two do not make four: Non-linear phenomena in ecology (The Croonian Lecture). Proc. R. Soc., Lond. B 228:241-266.

May, R. M. 1987. Chaos and the dynamics of biological populations. Proc. Royal Soc., Lond. A 413:27-44.

May, R. M. 1989. Detecting density dependence in imaginary worlds. Nature 338:16-17.

May, R. M., and G. F. Oster. 1976. Bifurcations and dynamics complexity in simple ecological models. Am. Nat. 110:573-599.

May, R. M., and T. R. E. Southwood. 1990. Introduction. Pages 1-22 IN B. Shorrocks and I. R. Swingland, eds. Living in a patchy environment. Oxford Univ. Press, Oxford. 246pp.

Pacala, S. W., and M. P. Hassell. in press. The persistence of host-parasitoid associations in patchy environments: II, evaluation of field data. Am. Nat. (in press).

*Perry, J. N. 1988. Some models for spatial variability of animal species. Oikos 51:124-130.

Ricker, W. E. 1954. Stock and recruitment. J. Fish. Res. Board, Can. 11:559-623.

Schaffer, W. M. 1985. Can nonlinear dynamics help us infer mechanisms in ecology and epidemiology? IMA Journal of

Mathematics Applied in Medicine and Biology 2:221-252.

Schaffer, W. M. 1988. Detecting order in the chaos of nature. Pages xxx-xxx in M. S. Boyce (ed.), Evolution of Life Histories of Mammals. Yale University Press, New Haven, CT.

Schaffer, W. M., and C. W. Tidd. 1991. NLF: Nonlinear forecasting for dynamical systems. Dynamical Systems, Inc., P.O. Box 35241, Tucson, AZ. 85740 USA.

Sugihara, G., and R. M. May. 1990. Nonlinear forecasting: An operational way to distinguish chaos from measurement error. Nature 344:734-741.

*Taylor, L. R. 1961. Aggregation, variance and the mean. Nature 189:732-735.

*Taylor, L. R. 1984. Assessing and interpreting the spatial distributions of insect populations. Ann. Rev. Entomol. 29:321-357.

*Taylor, L. R., Woiwood, I. P., and J. N. Perry. 1980. Variance and the large scale spatial stability of aphids, moths and birds. J. Anim. Ecol. 49:831-854.

*Thorarinsson, K. 1986. Population density and movement: a critique of delta-models. Oikos 46:70-81.

Turchin, P., and A. D. Taylor. 1992. Complex dynamics in ecological time series. Ecology (in press).

Wolda, 1975. Am. Nat.

Table 1. Effect of dispersal on dynamics of the 2-cell proportional dispersal model. Zones are demarcated on Figure 3.1.2

Zone	D	Characterization
1	0 - 0.034	transition from 2 chaotic asynchronous populations to 2-cycles; moves through region of quasi-periodic oscillations at D = 0.0213-0.034
2	0.034 - 0.176	2-cycles
3	0.22-0.8	subpopulations converge, behave as single population
4	0.8- 0.825	transition to equilibrium
5	0.825-0.967	equilibrium for both X_i and X_j.
6	0.967- 1.0	overcompensation in migration leading to chaos. At D=1, there is a total transfer of individuals between cells i and j.

~~20~~FIGURE CAPTIONS

Figure 2.1 The familiar Hopf bifurcation diagram of the Ricker model. Here 500 X values are plotted for each of 100 r values between 1 and 3.9 after 500 convergent iterations.

[from DS]

Figure 3.1.1 Maps of equation 2.2 with D = 0, and $r_i = r_j = 3.5$. Each subpopulation has its own 1-D map as in a, but there is no interaction between i and j such that the projection of $X_j(t+1)$ when plotted on $X_i(t)$ appears random as at b. Because of the overbearing structure illustrated in a, this carries over to a more complex structure in the 1-D map of the sum of the 2 populations at c. Further examples of these ΣX maps are plotted for $r_i = r_j = 2.9$ (d), 3.1 (e), 3.3 (f), 3.7 (g), 3.9 (h).

[get RICKER2.WK3 set D=0, r=3.5 plot MAPX2[X1], MAPSUM; then set r=2.9, 3.1, 3.3, 3.7, 3.9 and plot MAPSUM]

Figure 3.1.2 Coefficient of variation for X_i and ΣX as a function of the dispersal coefficient, D. Each plotted CV is calculated for 1,000 iterations of equation 2.2 with $r_i = r_j = 3.5$, $K_i = K_j = 1$, and initial $X_i = 0.5$, $X_j = 0.7$.

[get RICKER2.WK3 plot CV]

Figure 3.1.3 Lyapunov exponents for ΣX as a function of dispersal coefficient, D. Each value is calculated from 1,000 iterations of equation 2.2 as in the previous figure.

[to be calculated]

Figure 3.1.4 This sequence of ~~5~~ 6 maps explains how dispersal shapes the 1-D map of X_i and ΣX ~~from equation 2.2, with D = 0.02,~~ which ultimately determines the population's dynamics. In panel a we show the fundamental 1-D map of the Ricker model, i.e., $F(X_i)$, for $r_i = 3.5$, $K_i = 1.0$. The number of emigrants is simply $D*F(X_i)$ as plotted in panel b for a small value of D = 0.02. The residual population, then, before considering immigrants is $F(X_i) - D*F(X_i)$ plotted in c. The number of immigrants arriving from subpopulation j are calculated from a map like that at panel a, but here we assume no correlation between subpopulations. Therefore, the map of 1,000 points of $X_j(t+1)$ plotted as a function of $X_i(t)$ is messy but not random (panel d). Finally the sum of c (note the scale) and d completes the calculation of equation 2.2 for proportional dispersal, plotted in panel e, and the sum of the 2 populations mapped in panel f.

[get RICKER4.WK3, set D=.02, plot FIG31A, FIG31B, FIG31C]
[get RICKER2.WK3, set D=.02;r=3.5,3.5;K=1,1, plot MAPX2[X1], MAPX1, MAPSUM]

Figure 3.1.5 At $0.0244 < D < 0.02514$ we observe the emergence of an 18-point cycle of abundance for each subpopulation and a 9-point cycle for the total population. Here we plot the 1-D map for the ΣX with $D = 0.0245$ (a), as well as a brief segment of the time series (b).

[get RICKER2.WK3 set D=0.0245, plot SUMMAP, TIMELATE]

Figure 3.1.6 Quasi-periodic oscillations occur in the vicinity of $0.02514 < D < 0.034$ resulting in attractive maps. Panel a shows the portions of the map of X_i where all motion occurs. When combined with X_j's map at b, and resultance dispersal movements at d, we obtain the map of ΣX plotted in panel ~~d~~. e Each subpopulation is oscillating with approximately equal magnitude as shown by the phase diagram in panel ~~e~~. c. For each of these plots, $D = 0.03$, $r_i = r_j = 3.5$, initial $X_i = 0.5$, $X_j = 0.7$, and 1,000 iterations were performed.

[get RICKER2.WK3 set D=0.03, plot MAPX1, MAPX2[X1], MAPDIFFS, MAPSUM, PHASE]

Figure 3.1.7 At $D = 0.035$, each subpopulation converges on a 2-cycle, and the total population mapped here converges on equilibrium.

[get RICKER2.WK3 set D=.035, plot MAPSUM]

Figure 3.1.8 Abruptly at $D = 0.177$, we emerge from equilibrium with the emergence of familiar structure not only in the 1-D map of X_i (a), but very similar shape in the 1-D map of ΣX c (~~b~~). A 1-D map of the differences shows a curious shape in panel d. The phase plot for the 2 subpopulations appears to take on a cigar shape at ~~d~~. b. Intermittency in dynamic behavior is common in this transition phase as illustrated by the time series of X_i for $D = 0.178$ plotted in panel e.

[get RICKER2.WK3 set D=.177, plot MAPSUM, MAPX1, MAPDIFFS, PHASE; set D=0.178, plot TIMEX1]

Figure 3.1.9 Dispersal begins to drive the 2 subpopulations to convergence in dynamics. Here, for $D = 0.21$, the time series of the number of dispersers shows sudden bursts of activity, but nearly convergence dynamics most of the time (a). The phase diagram (b) is nearly an isometric line.

[get RICKER2.WK3 set D=0.21, plot TIMEDIFFS, PHASE]

Figure 3.1.10 For $0.22 < D < 0.79$, both subpopulations take on identical synchronous dynamics, and this 1-D map for ΣX characterizes the dynamics for the population as a whole.

[get RICKER2.WK3 set D=.22, plot MAPSUM]

Figure 3.1.11 Bursts of activity in dispersal between X_i and X_j

appear for D = 0.8, as synchrony in chaos begins to break down.

[get RICKER2.WK3, set D=.8, plot TIMEDIFFS]

Figure 3.1.12 Convergence towards equilibrium for the 2 subpopulations can be first seen when dispersers begin to show intermittent periods moving in either one direction or another, seen in panel a for D = 0.82. This is also reflected in the population time series as well (b). The development of two critical points at X_i = 0.5 and 2.38 is further seen in the 1-D map plotted in c. For subpopulation i we see the time series lock into the lower stable point with convergence going to equilibrium of X_i=0.5 illustrated in the time series at b, d and e, ~~and h~~, and the maps at c, f, ~~and i~~.

[get RICKER2.WK3, set D = 0.82, 0.825, 0.83; plot TIMEDIFFS, TIMEX1, MAPX1]

Figure 3.1.13 One-dimensional map of ΣX for D = 0.825 showing the emergence of a stable equilibrium at ΣX = 2.88.

[get RICKER2.WK3, set D = 0.825, plot MAPSUM]

Figure 3.1.14 Bifurcation map on D for the 2-cell proportional dispersal model with $r_i = r_j = 3.5$ and $K_i = K_j = 1.0$. Also refer to Fig. 3.1.2 and 3.1.3.

[calculate with DS]

Figure 3.1.15 Coefficient of variation in population size for X_i, X_j, and ΣX as a function of D in the 2-cell proportional dispersal model where $r_i = 3.5$, $r_j = 2.7$, $K_i = K_j = 1$. Asymmetry is attributable to asymmetry in r values.

[get RICKER2.WK3, plot CV2.7]

Figure 3.1.16 Bifurcation diagram corresponding to previous figure.

[from DS]

Figure 3.1.17 Coefficient of variation in population size for X_i, X_j, and ΣX as a function of D in the 2-cell proportional dispersal model where $r_i = 3.5$, $r_j = 2.0$, $K_i = K_j = 1$.

[get RICKER2.WK3, plot CV2.0]

Figure 3.1.18 Bifurcation diagram corresponding to the previous figure.

[from DS]

Figure 3.1.19 Coefficient of variation in population size for X_i,

X_i, and ΣX as a function of D in the 2-cell proportional dispersal model where $r_i = 3.5$, $r_j = 1.0$, $K_i = K_j = 1$.

[get RICKER2.WK3, plot CV1.0]

Figure 3.1.20 Bifurcation diagram corresponding to the previous figure.

[from DS]

Figure 3.1.21 Here K is different in each of the 2 cells with $K_i = 1.0$, and $K_j = 2.0$, but with $r_i = r_j = 3.5$. Each point is based upon projections for 1,000 time periods with initial $X_i = 0.5$ and $X_j = 0.7$.

[get RICKER2.WK3, plot CVK2]

Figure 3.2.1 Coefficient of variation for X_i and ΣX as a function of the dispersal coefficient, D, for the 2-cell density-dependent dispersal model with $r_i = r_j = 3.5$, $K_i = K_j = 1$. Each point is based upon projections for 1,000 time periods with initial $X_i = 0.5$ and $X_j = 0.7$.

[get RICKER3.WK3, plot CV]

Figure 3.2.2 Plot of the phase space for density-dependent dispersal with large D = 0.25. Based upon 1,000 points with parameter values set as described in the caption to the previous figure.

[get RICKER3.WK3, set D=.25, plot phase]

Figure 3.2.3 The 1-D map for X_i corresponding with the previous figure. The large values occurring in the vicinity of the peak of the map eventually destabilize the system.

[get RICKER3.WK3, set D=.25, plot MAPX1]

Figure 3.2.4 Bifurcation diagram corresponding to Fig. 3.2.1.

[from DS]

Figure 4.1 CV for X_5 and ΣX as a function of D for the dispersal pool model.

[get RICKPOOL.WK3, plot CV]

Figure 4.2 CV for X_5 and ΣX as a function of D for the 9-cell linear chain model.

[get RICK~~???~~5x9.WK3, plot CV]

Figure 4.3 CV for X_5 and ΣX as a function of D for the 9-cell grid.

[get RICKGRID.WK3, plot CV]

Figure 5.1 CV for X_5 and ΣX as a function of D for the 9-cell ring model.

Figure 6.1.1 The forecasting "signature" of chaos, plotted for 3 different epsilon values. In resource exploitation applications, we suspect that epsilon will assume relatively large values. For example, accomplishing population estimation within 10% of the actual values ($\epsilon = 0.1$) would be exceptionally good.

Figure 6.1.2 Coefficient of determination as a function of forecast interval for X_i in the 2-cell proportional dispersal model with D = 1.

Figure 6.1.3 Decay of forecasting ability with increasing D over the range of D=0 to D=...

Figure 6.1.4 Carrying on from the previous figure, bringing D into the region of periodic behavior. As the projections become quasi-periodic, we see the right tail of the forecast signature lift until ultimately perfect forecasting occurs when X_i is periodic.

Figure 6.2.1 Forecasting ability of a global model based upon r = 3.5 when applied to populations projected from various r values. Presented are the coefficient of determination (r^2), sums of squares, and mean deviance between 1-time period predictions and observed. Assumes no dispersal and K's = 1.

* ~~[get FORECAST.WK3, plot xxx]~~

Figure 6.2.2 Forecasting ability where K is allowed to vary. Mean deviance increases approximately exponentially as K is increased or decreased from the original value of 1.0.

* ~~[get FOREK, plot xxx]~~

Figure 6.3.1 Forecast interval plot for a population in a relatively broad periodic region of parameter space. Here the model is a 2-cell proportional dispersal model as in §3.2 with D = 0.1, $r_i = r_j = 3.5$. Noise is incorporated multiplicatively with ± bounds at 0.15, 0.5 and 0.9. Without noise, forecasting is perfect, i.e., $r^2 = 1.0$ for all projected intervals.

* ~~[get INTERVAL.WK3, plot D.1]~~ olo legends.

Figure 6.3.2 As in previous figure except D = 0.0245. Without noise the population has an 18-cycle, but over a narrow range of D values.

[get INTERVAL.WK3, plot D.025]

Figure 6.4.1 Time series for 2-cell proportional dispersal model with D = 0.178, r_i = r_j = 0.178, K_i = K_j = 1.0 showing intermittency in dynamics for X_i, moving between quasi-periodic oscillations and chaos.

[get RICKER2.WK3, set D = 0.178, plot TIMEX1, TIMESUM]

Figure 6.4.2 One-dimensional maps for the 2 time series illustrated in Fig. 6.4.1.

[get RICKER2.WK3, set D = 0.178, plot MAPX1, MAPSUM]

Figure 6.4.3 Coefficient of determination as a function of forecast interval for local nonlinear forecasts of the time series presented in Fig. 6.4.1. Note that forecasts are actually better for the more chaotic ΣX than for the intermittent X_i time series. In both cases, local region epsilons equal 0.1.

[get FORE178.WK3, plot X1-SUMX]

Figure 6.5.1

Figure 6.5.2 Predicted and observed values for a global forecasting model based upon r = 3.5, applied to a time series from r = ... Characterizing this relationship with r^2 clearly violates assumptions of linearity and homogeneity of variances.

Figure 6.5.3 Predicted and observed values plotted for a Ricker model iterated with r = 2.8, using a local forecasting model (Schaffer and Tidd 1990). Separation of successive iterations between high and low values yields spuriously high values of r^2 suggesting higher accuracy of prediction than is realized.

[to be generated from DS predicted/observed plot showing separation of points]

Figure 6.6.1 Metapopulation forecasting for 2-celled Ricker model projections with subpopulations out of phase and D=0, r_i=r_j, K_i=K_j=1 based upon an axis of 200 points used to forecast the next 800 points. Convergent iterations were calculated for 500 time periods prior to beginning forecast model construction. Values plotted are the coefficients of determination (r^2) of the relationship between predicted and observed values for the 800 points.

[get INTERVAL.WK3, plot META29]

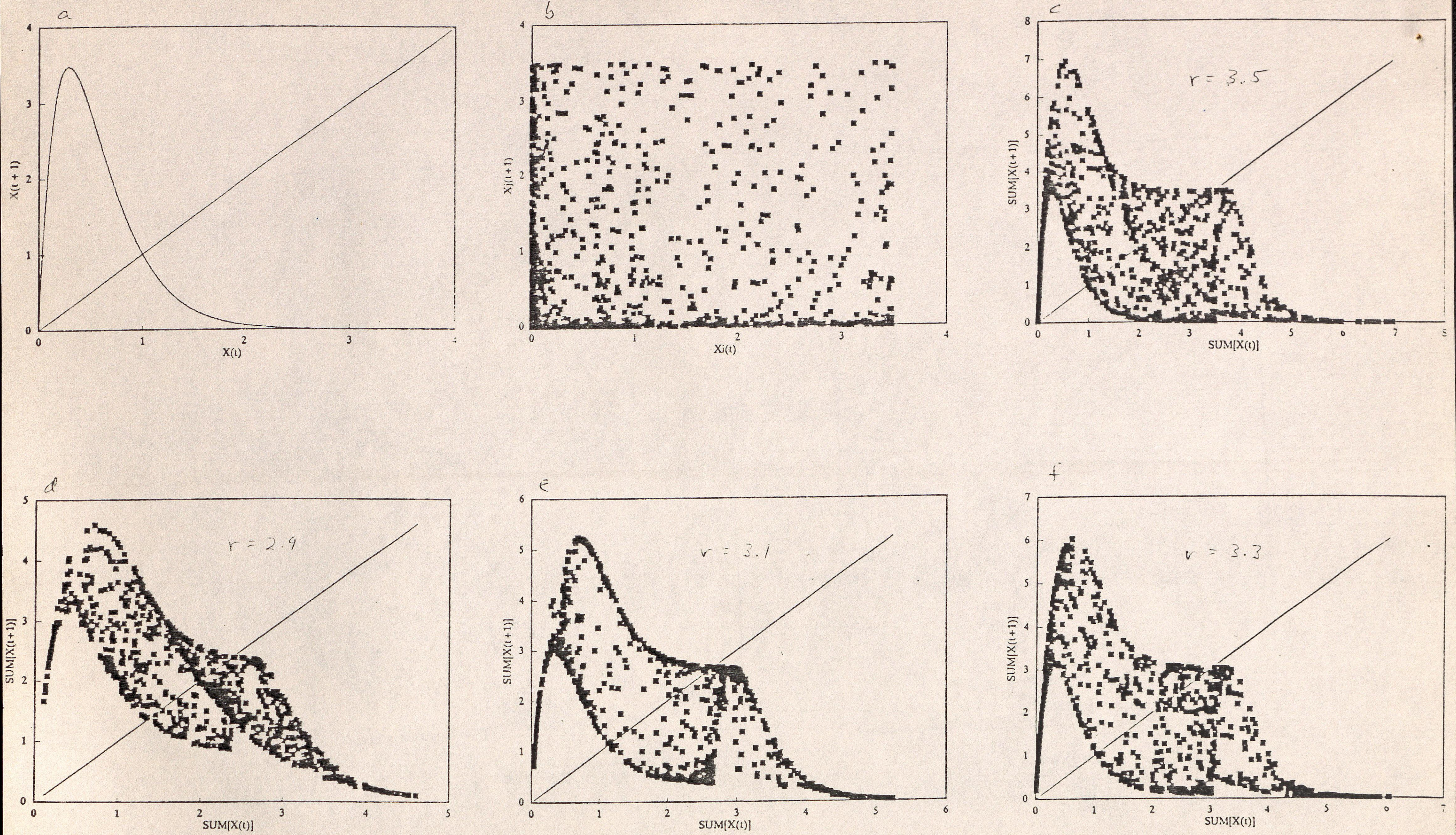

a
X(t + 1)
X(t)
b
Xj(t + 1)
Xi(t)
c
r = 3.5
SUM[X(t+1)]
SUM[X(t)]
d
r = 2.9
SUM[X(t+1)]
SUM[X(t)]
e
r = 3.1
SUM[X(t+1)]
SUM[X(t)]
f
r = 3.3
SUM[X(t+1)]
SUM[X(t)]

Fig. 3.1.1

g

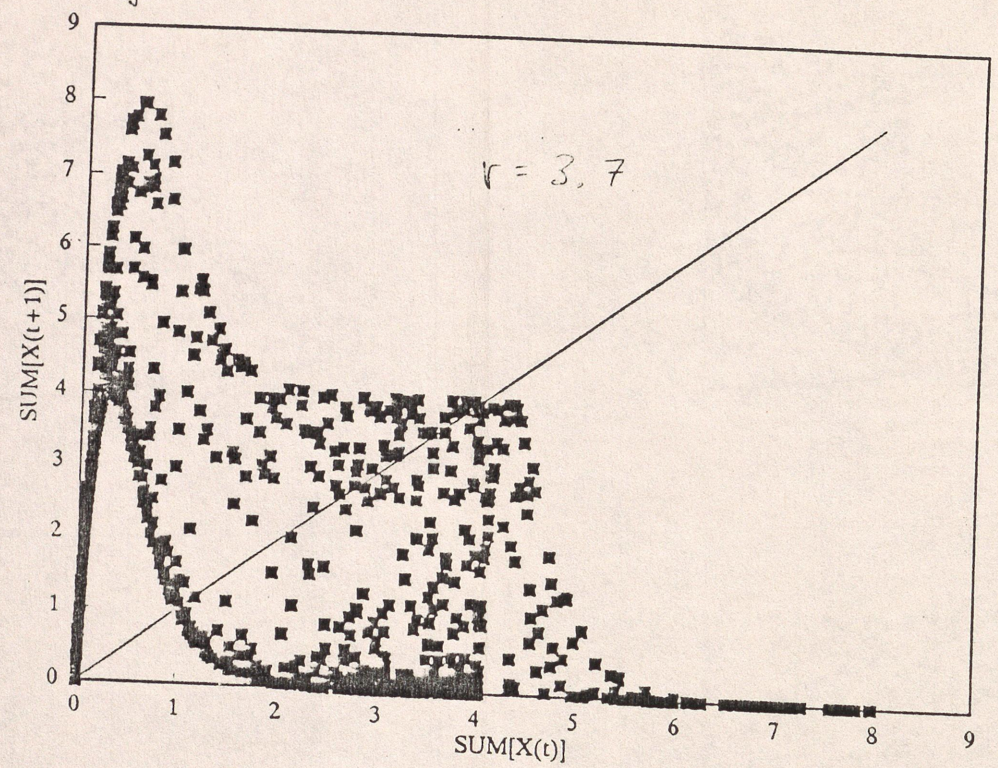
r = 3.7
SUM[X(t+1)]
SUM[X(t)]
0
1
2
3
4
5
6
7
8
9

h.

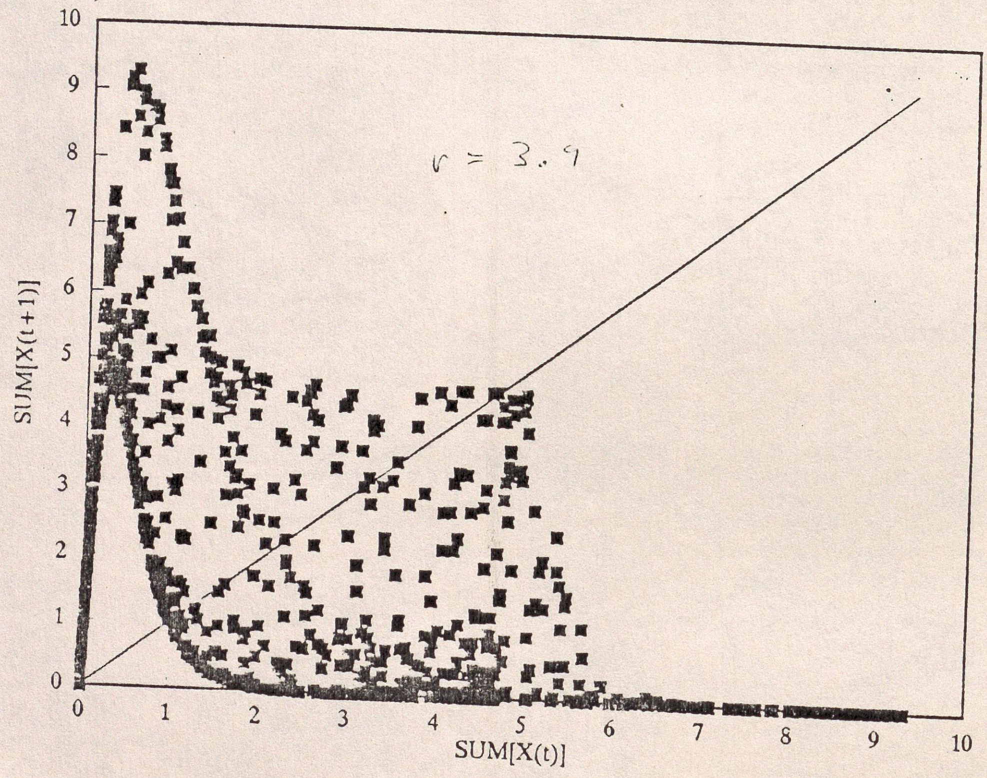
r = 3.9
SUM[X(t+1)]
SUM[X(t)]
0
1
2
3
4
5
6
7
8
9
10

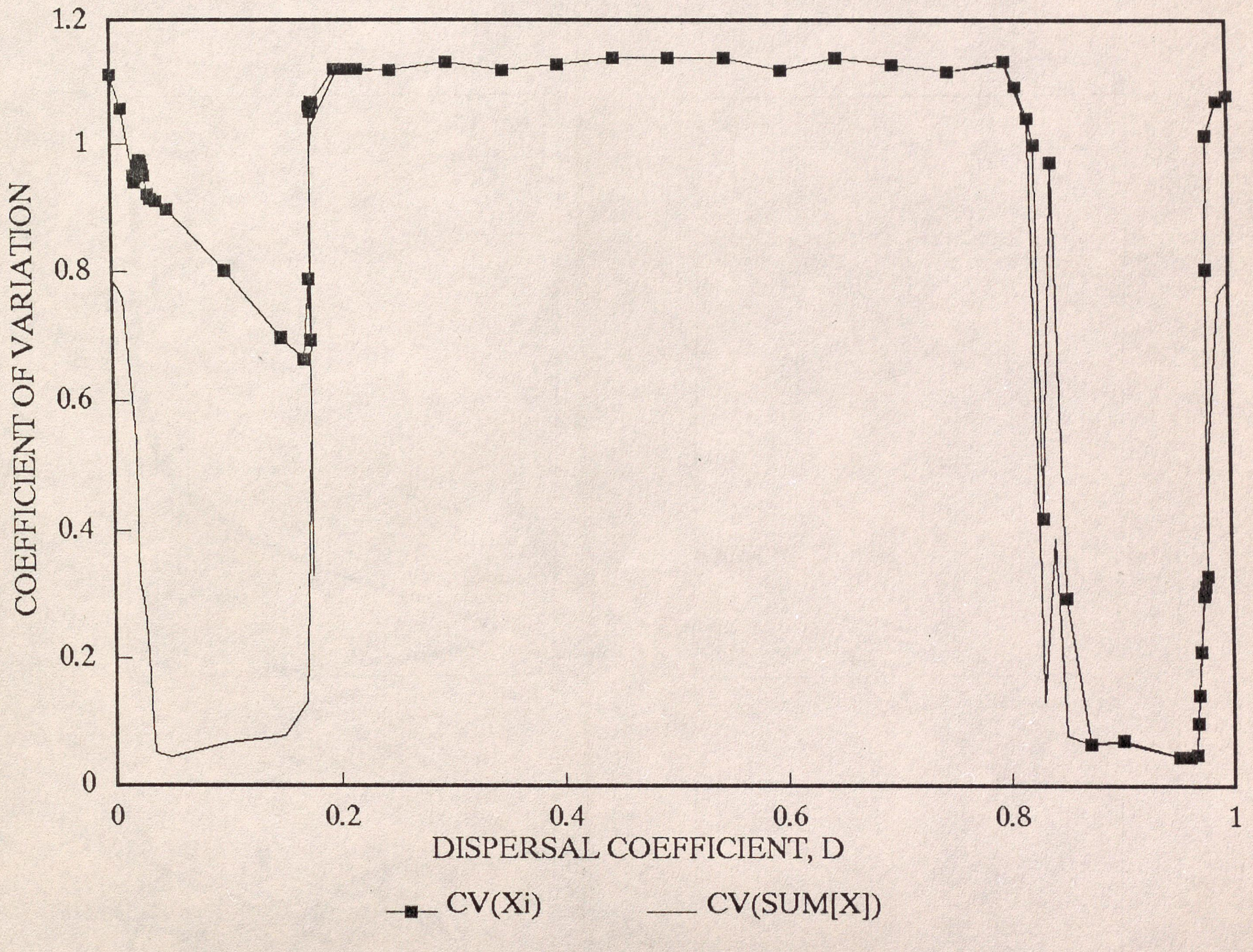
1.2
1
0.8
0.6
0.4
0.2
0
COEFFICIENT OF VARIATION
0
0.2
0.4
0.6
0.8
1
DISPERSAL COEFFICIENT, D
CV(Xi)
CV(SUM[X])

Fig 3.1.2

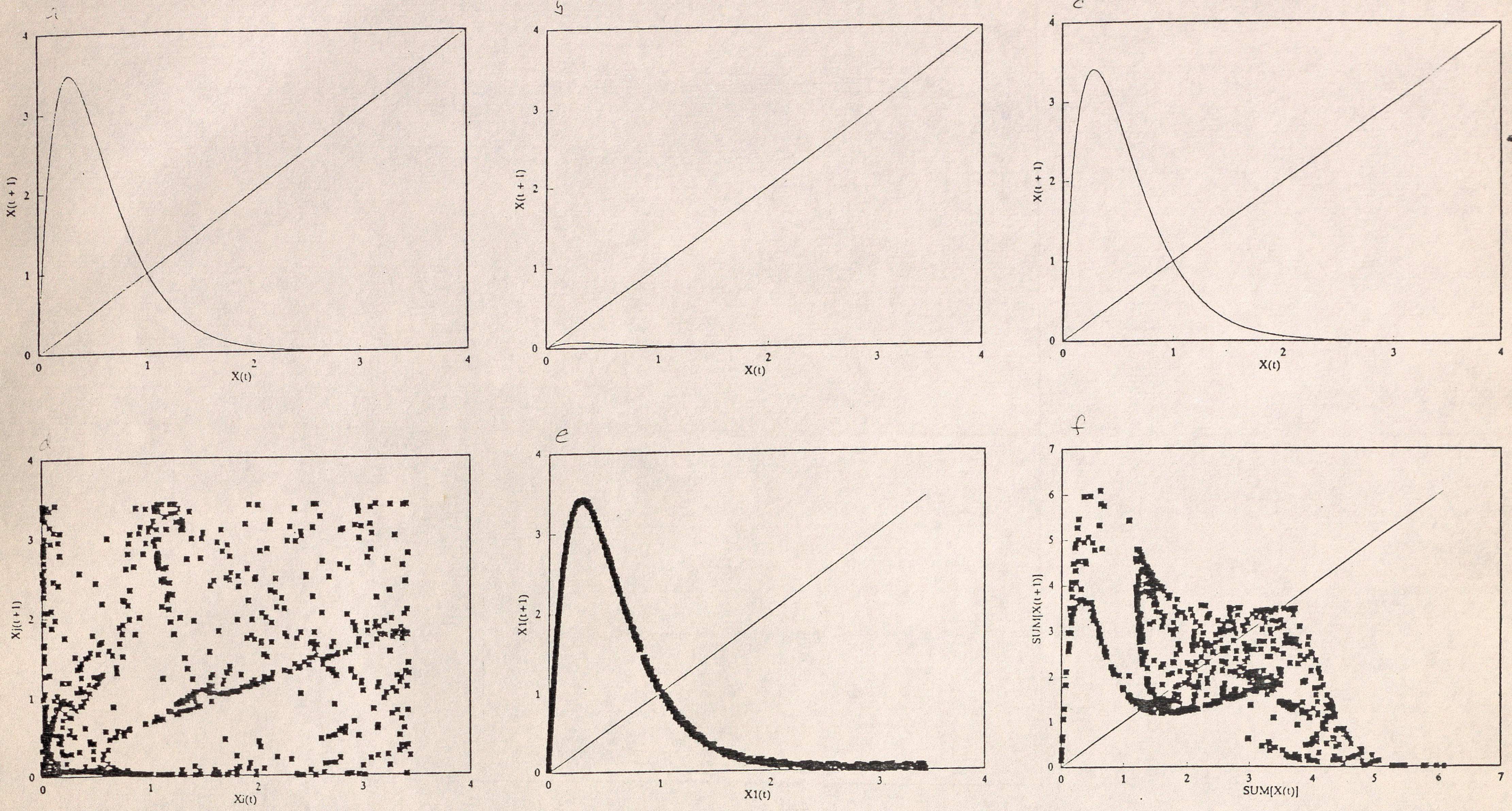

Fig 3.1.4

Fig. 3.15

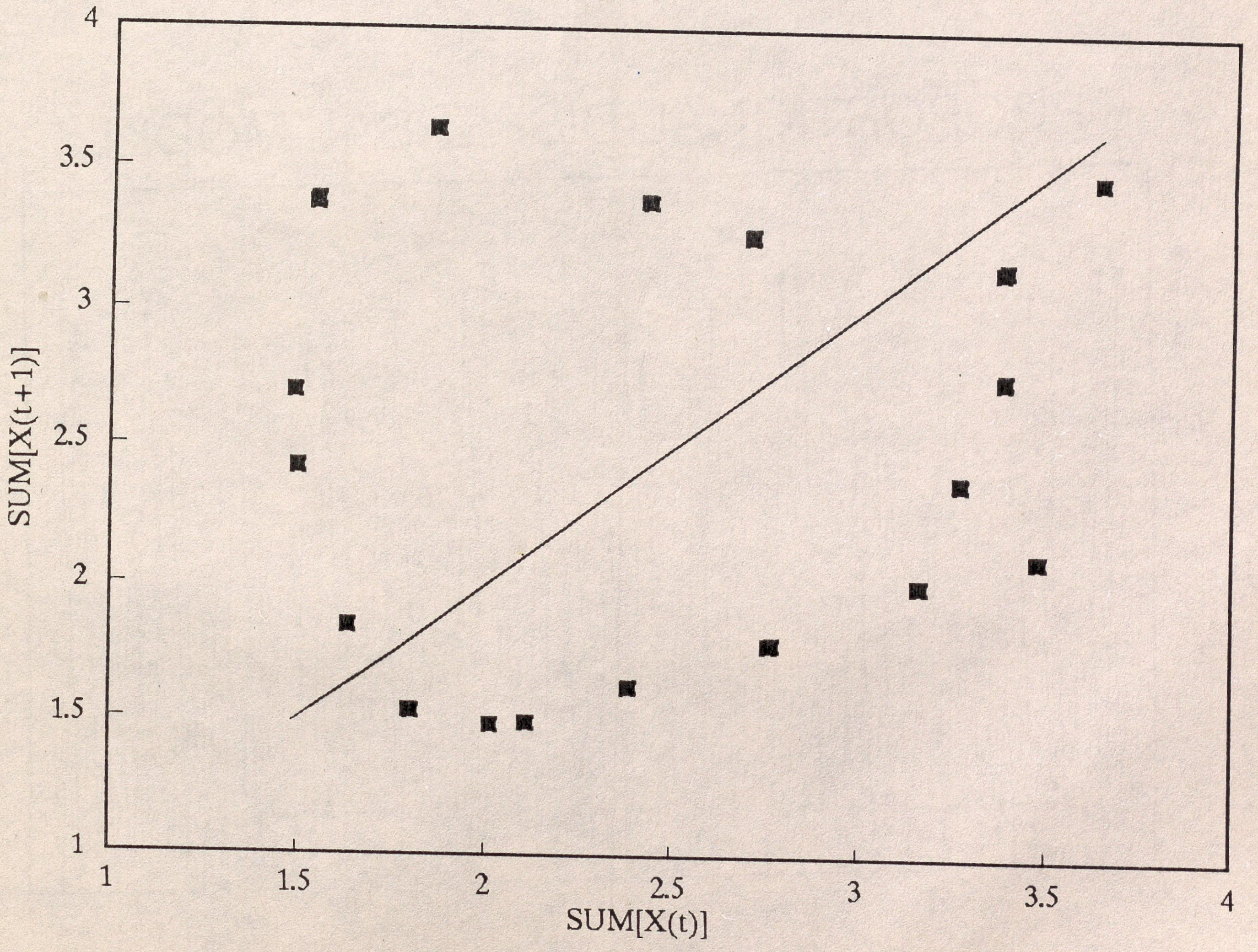

3,1.56

PROPORTIONAL DISPERSAL MODEL

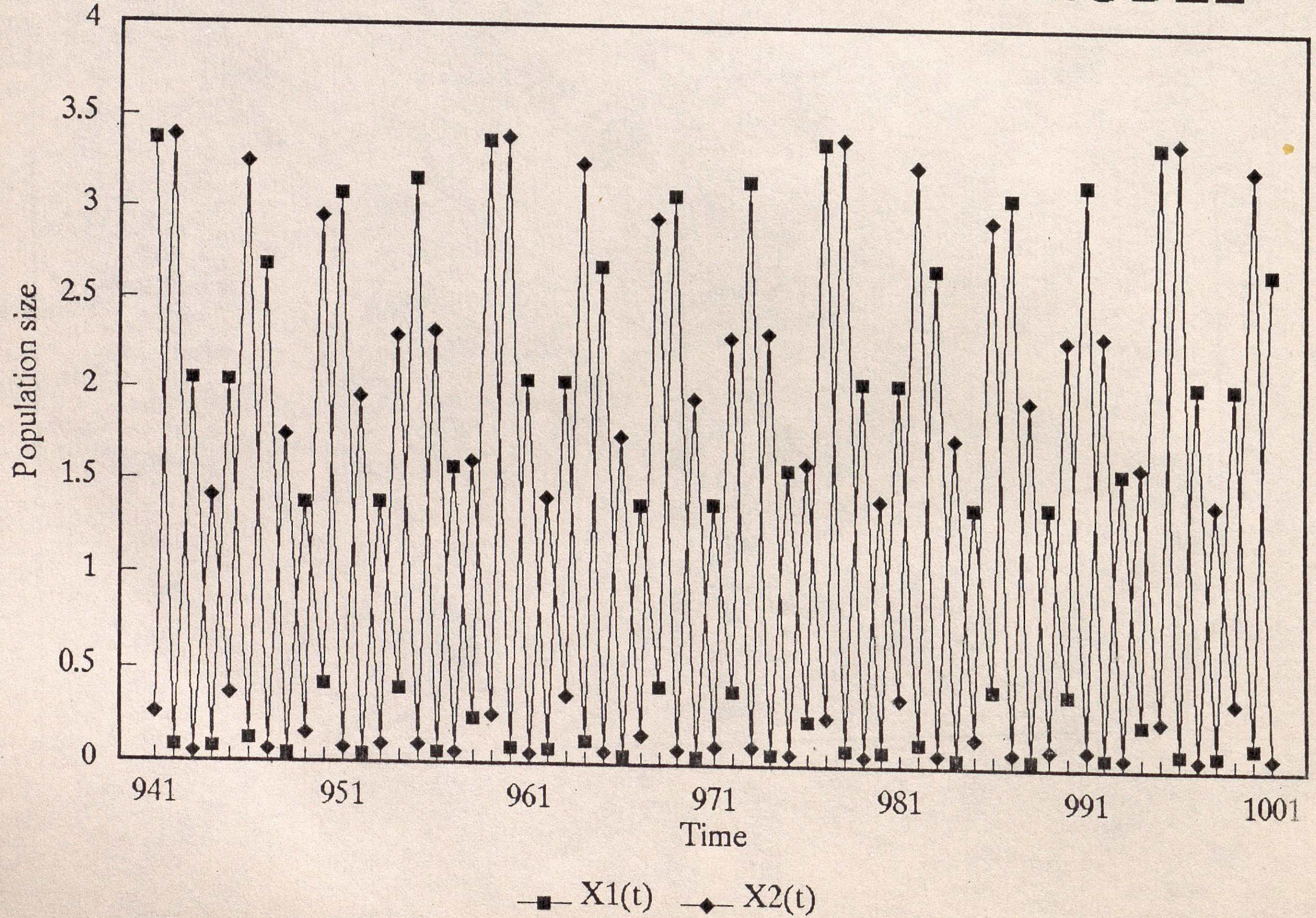

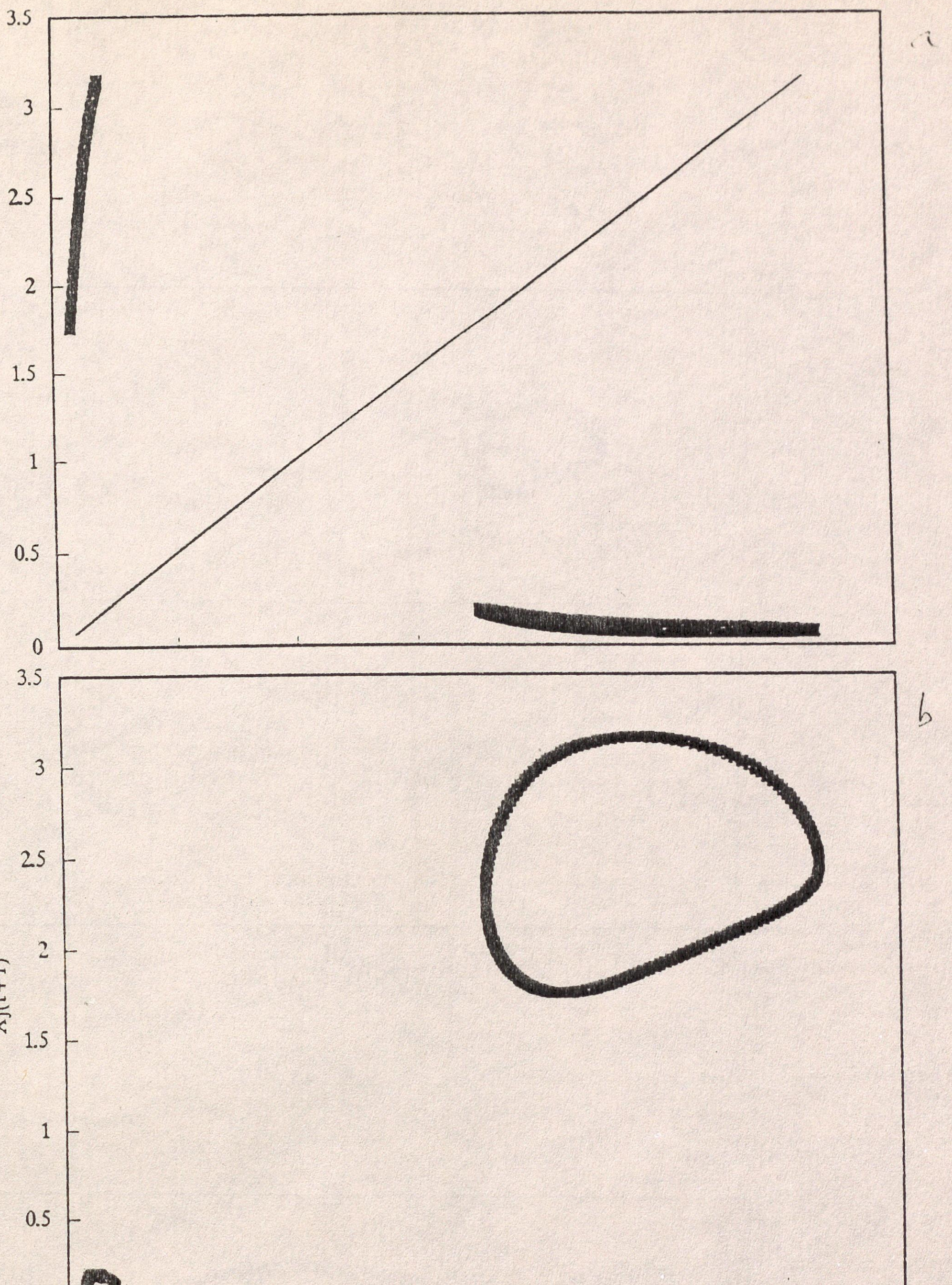

Fig. 3.1.6

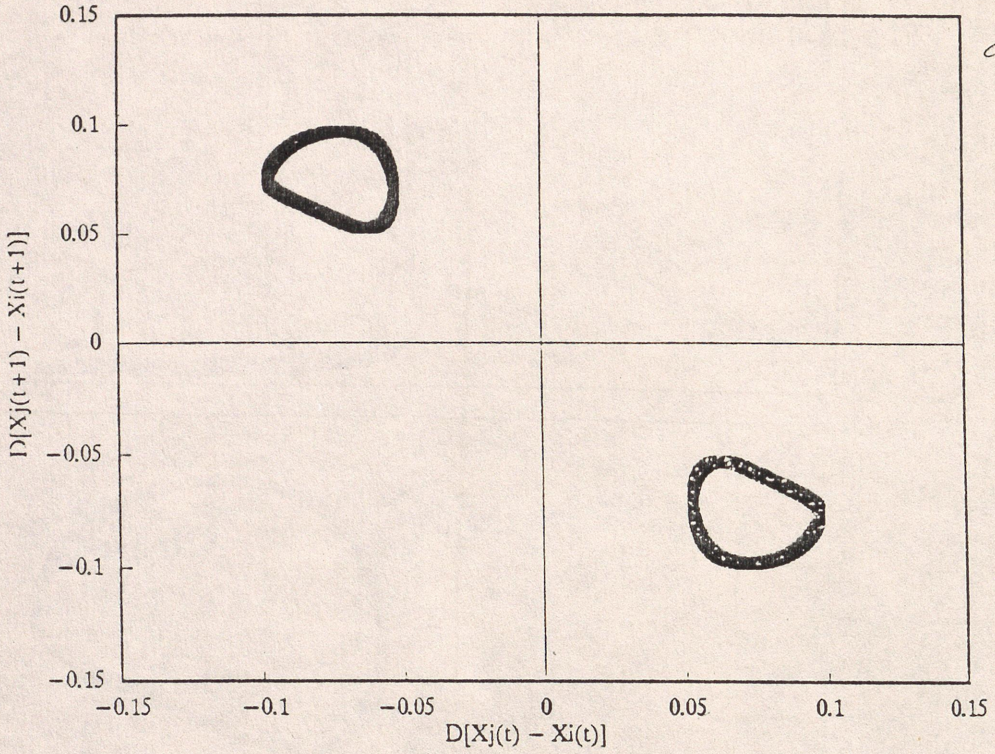

0.15
0.1
0.05
0
−0.05
−0.1
−0.15
D[Xj(t+1) − Xi(t+1)]
−0.15
−0.1
−0.05
0
0.05
0.1
0.15
D[Xj(t) − Xi(t)]

d

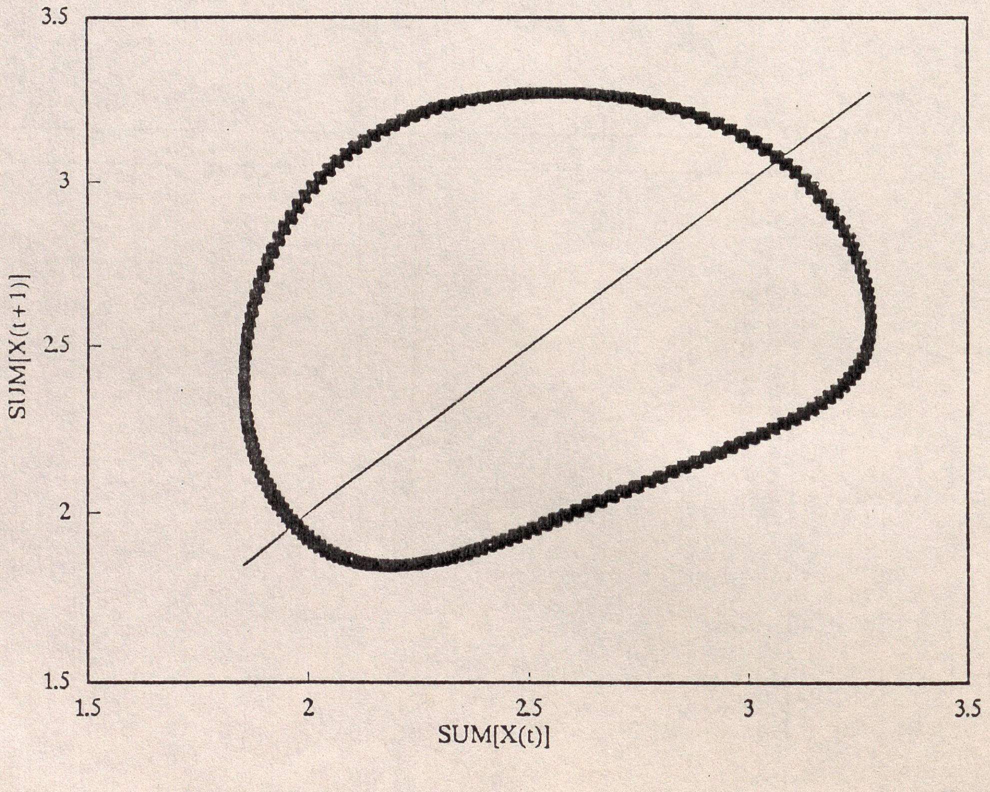

3.5
3
2.5
2
1.5
SUM[X(t+1)]
1.5
2
2.5
3
3.5
SUM[X(t)]

e

3.1.6

Fig. 3.1.7

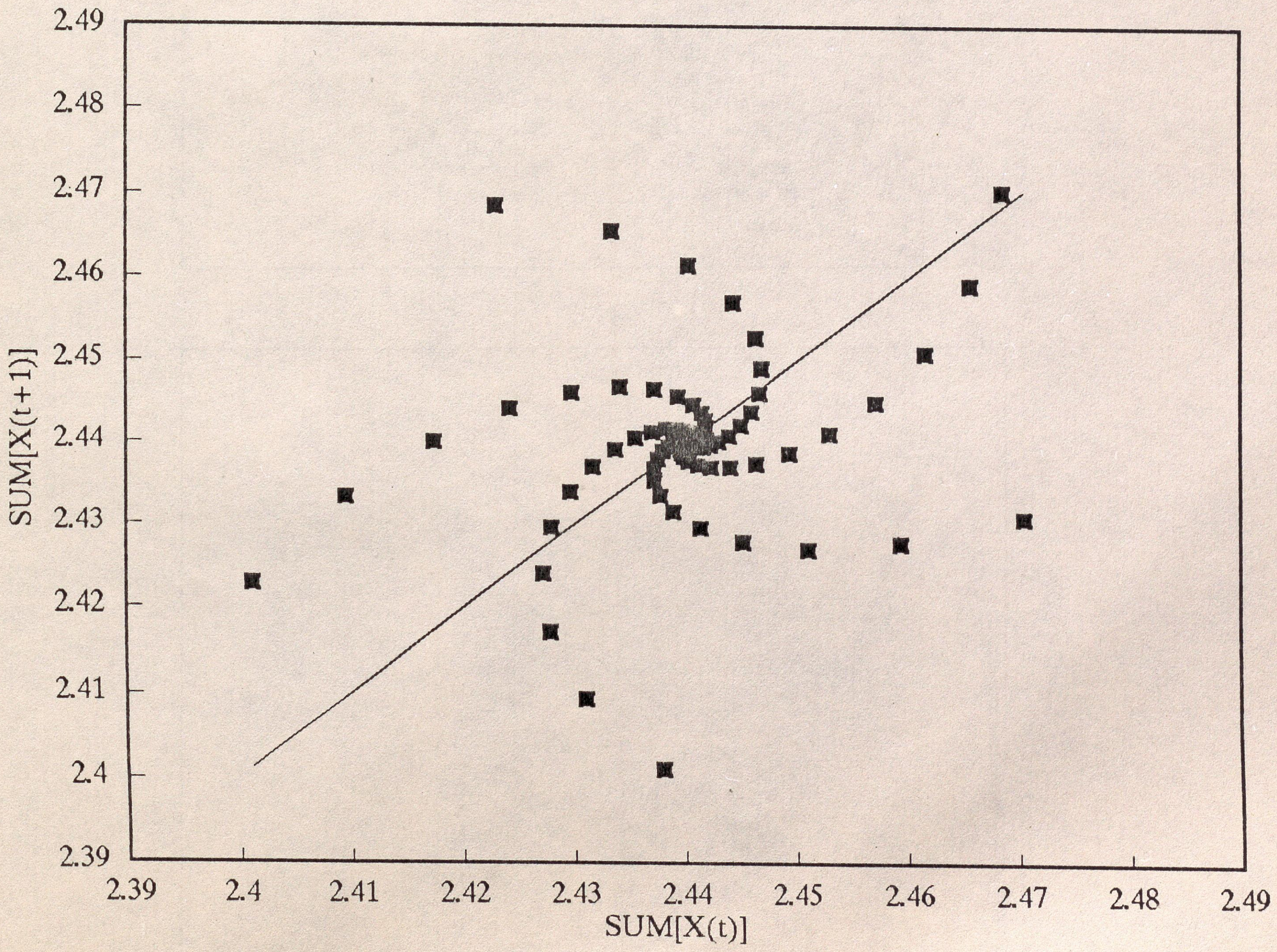

2.49
2.48
2.47
2.46
2.45
2.44
2.43
2.42
2.41
2.4
2.39
SUM[X(t+1)]
2.39
2.4
2.41
2.42
2.43
2.44
2.45
2.46
2.47
2.48
2.49
SUM[X(t)]

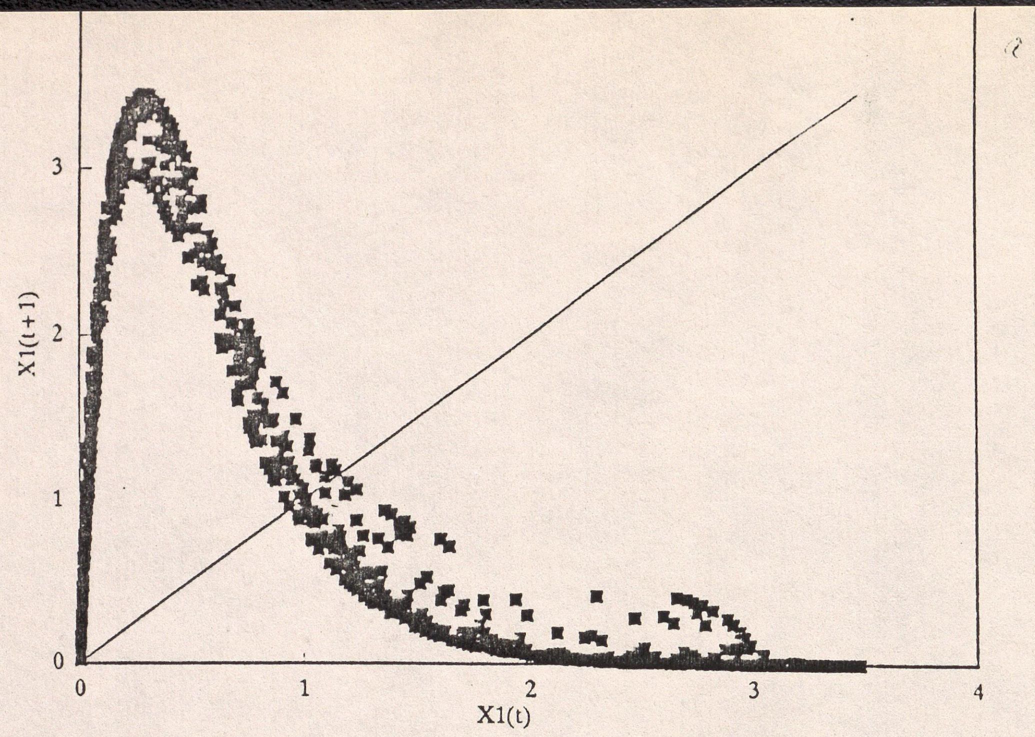

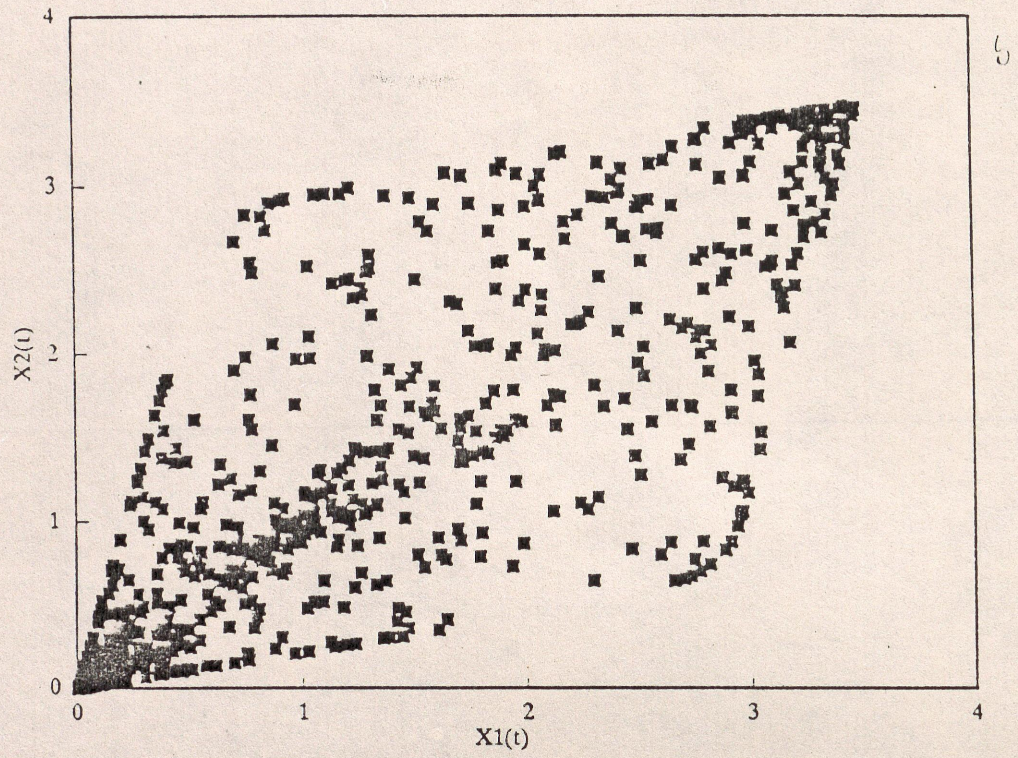

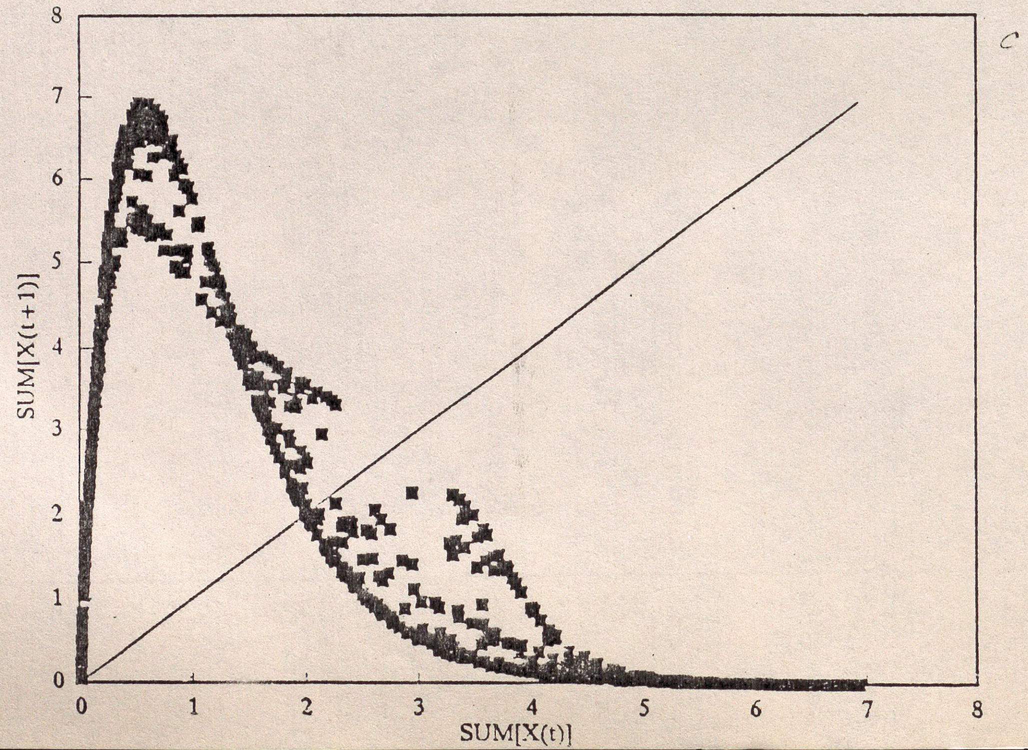

3.1.8

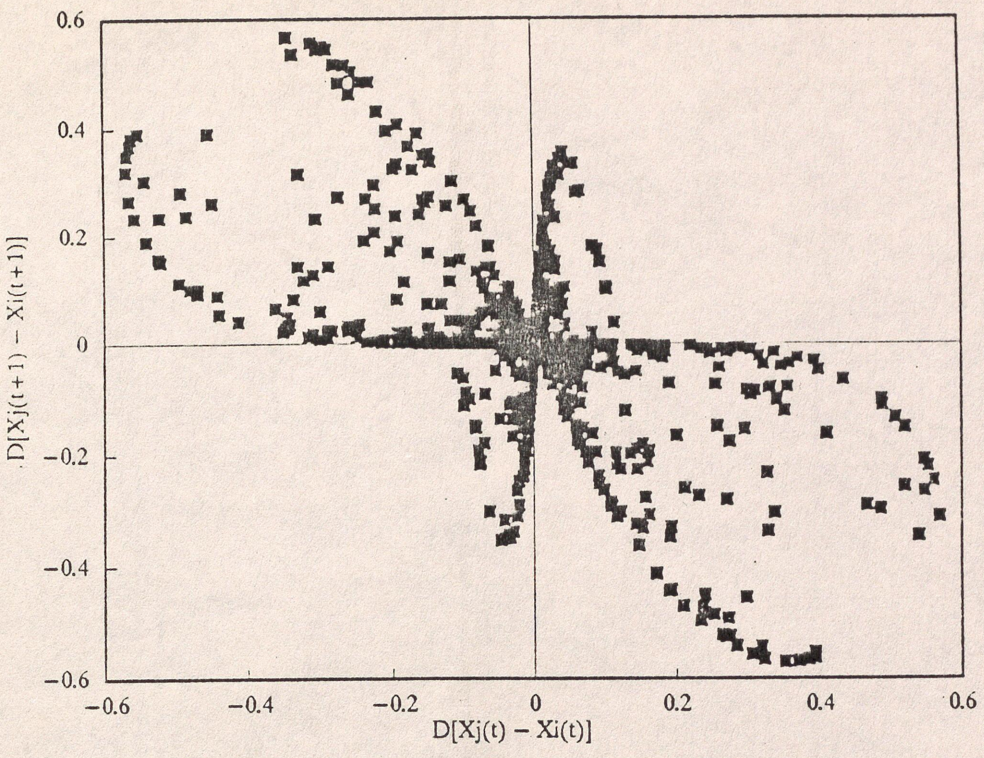

d

Dispersal Model Time Series

e

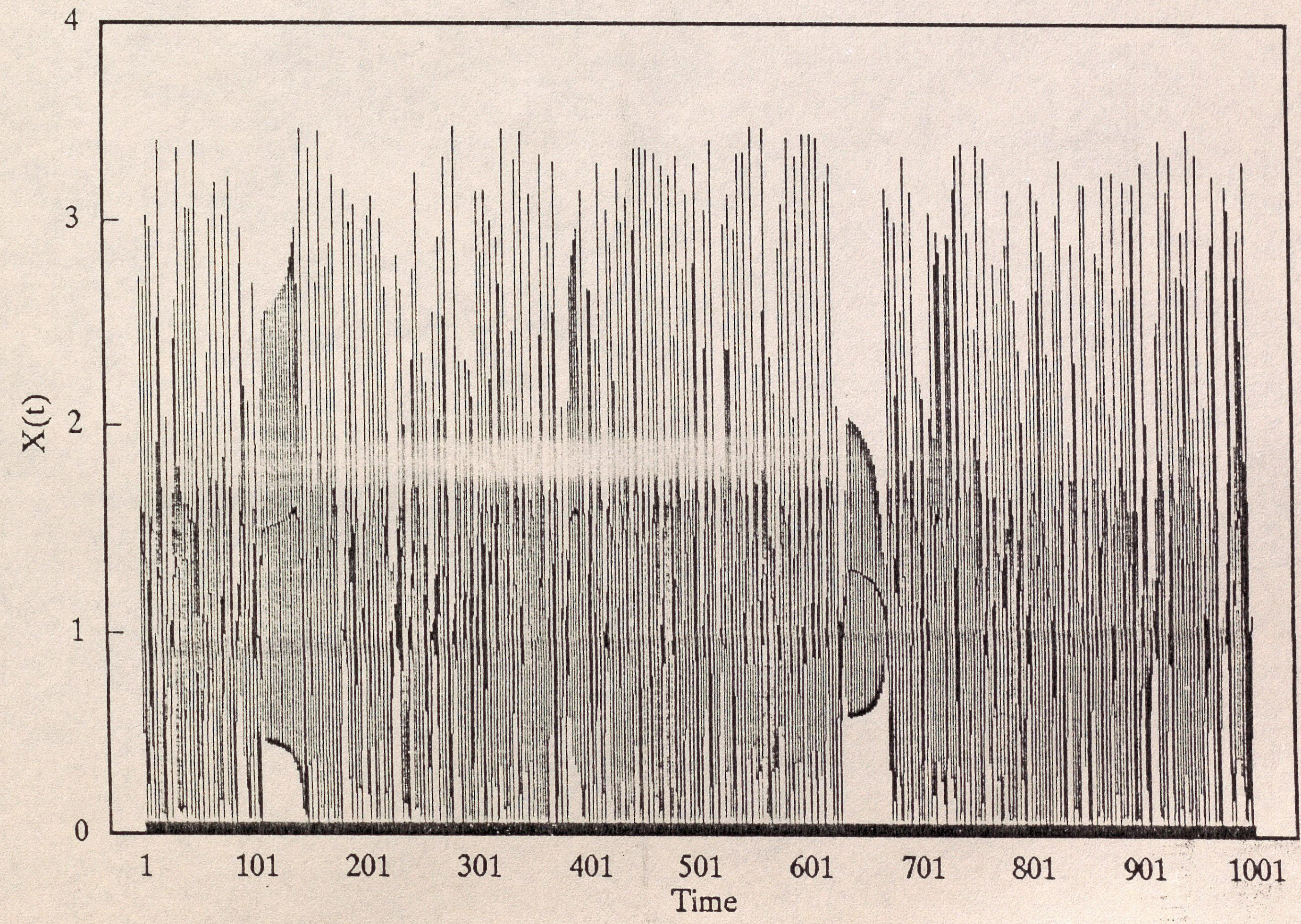

3.1.8

Time Series of Dispersal

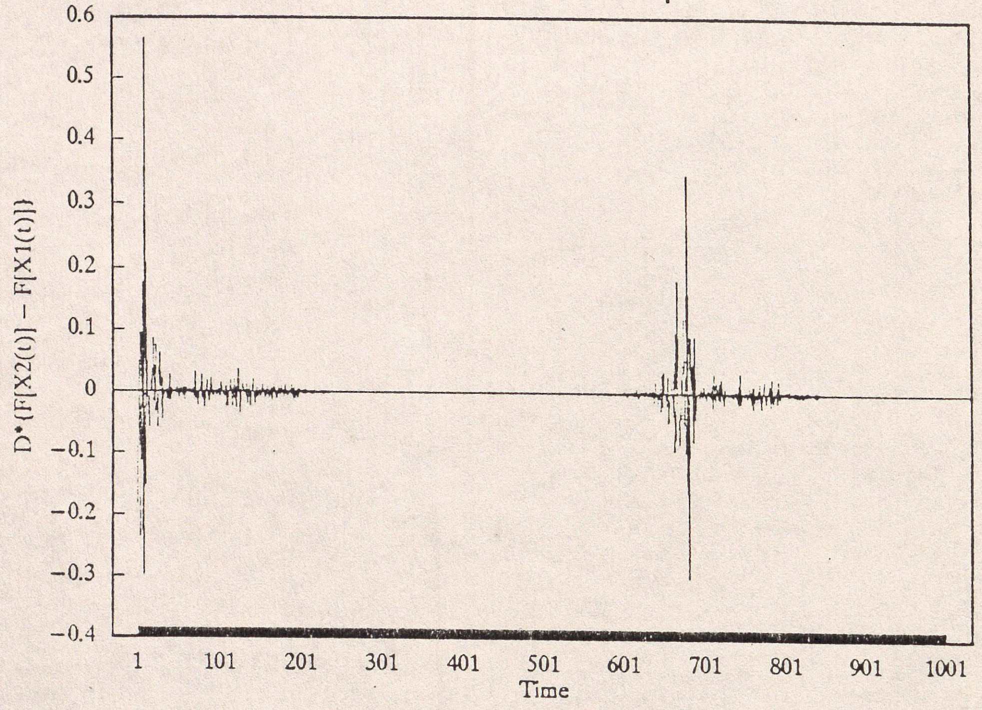

a

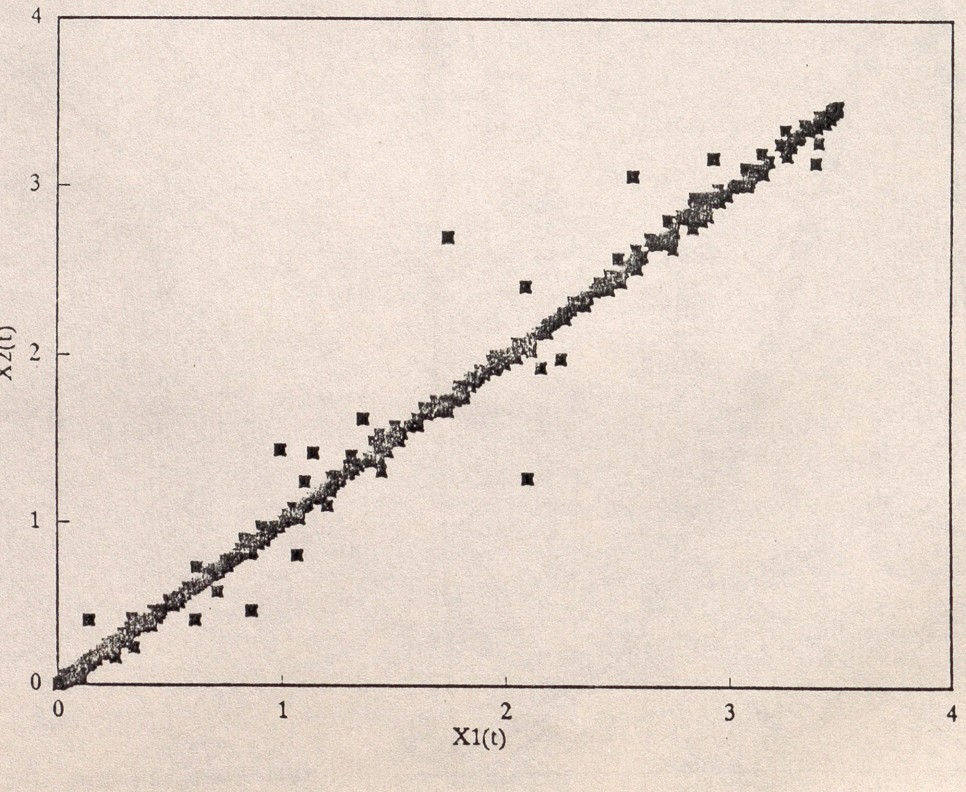

b

Fig 5.19

Fig 3.1.10

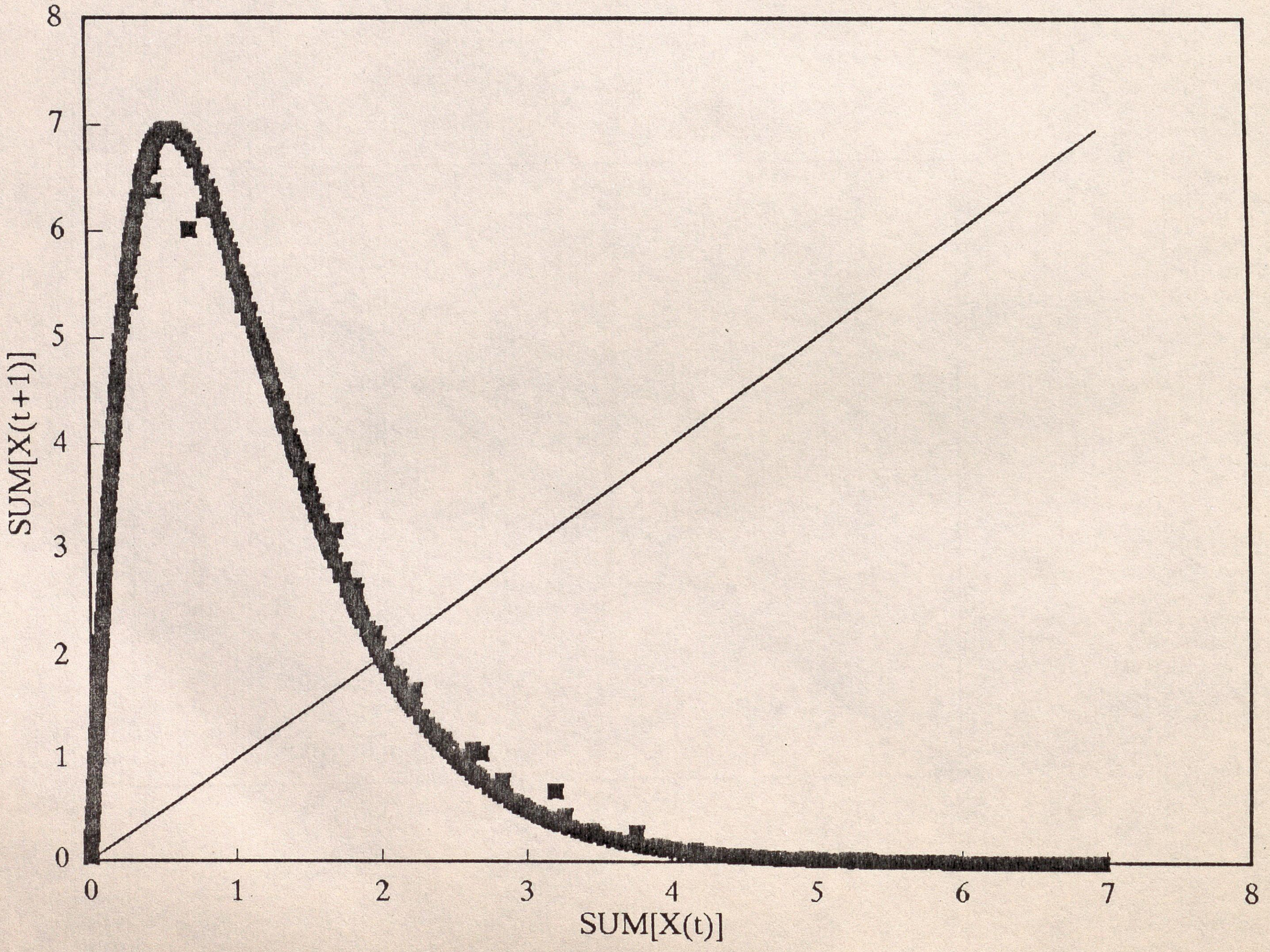

Fig 3.1.11

Time Series of Dispersal

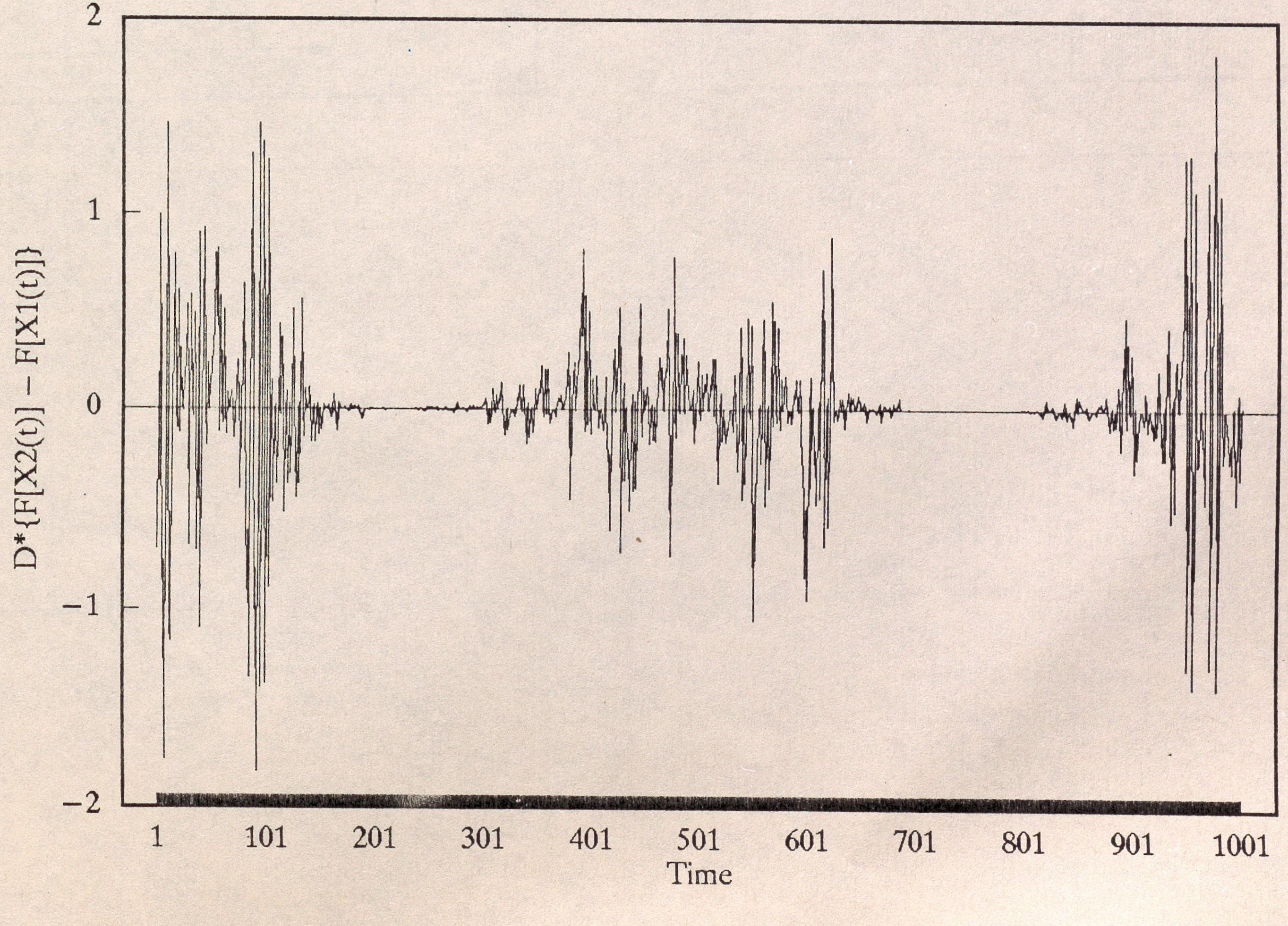

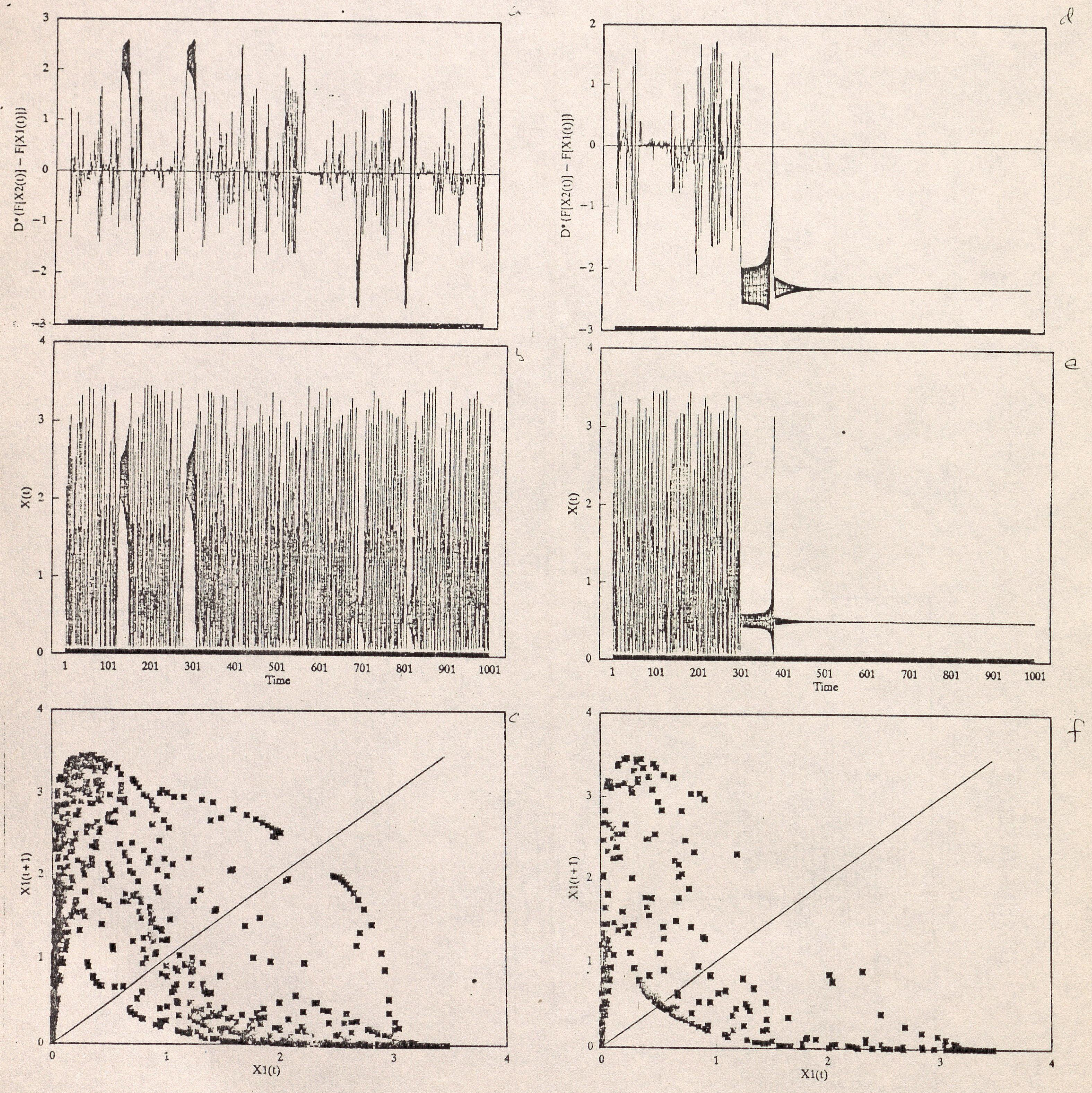

Fig. 3.1.12

3.113

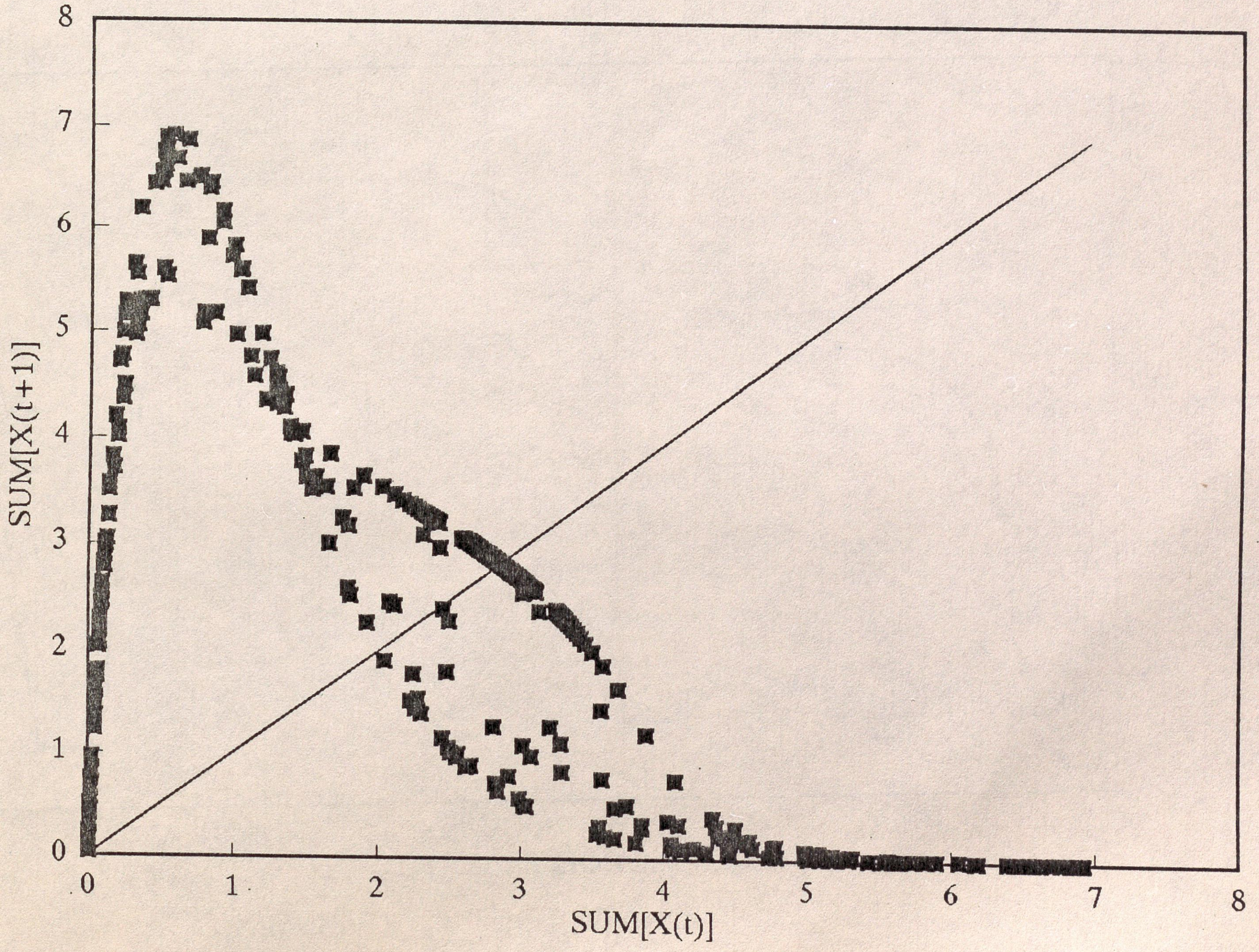

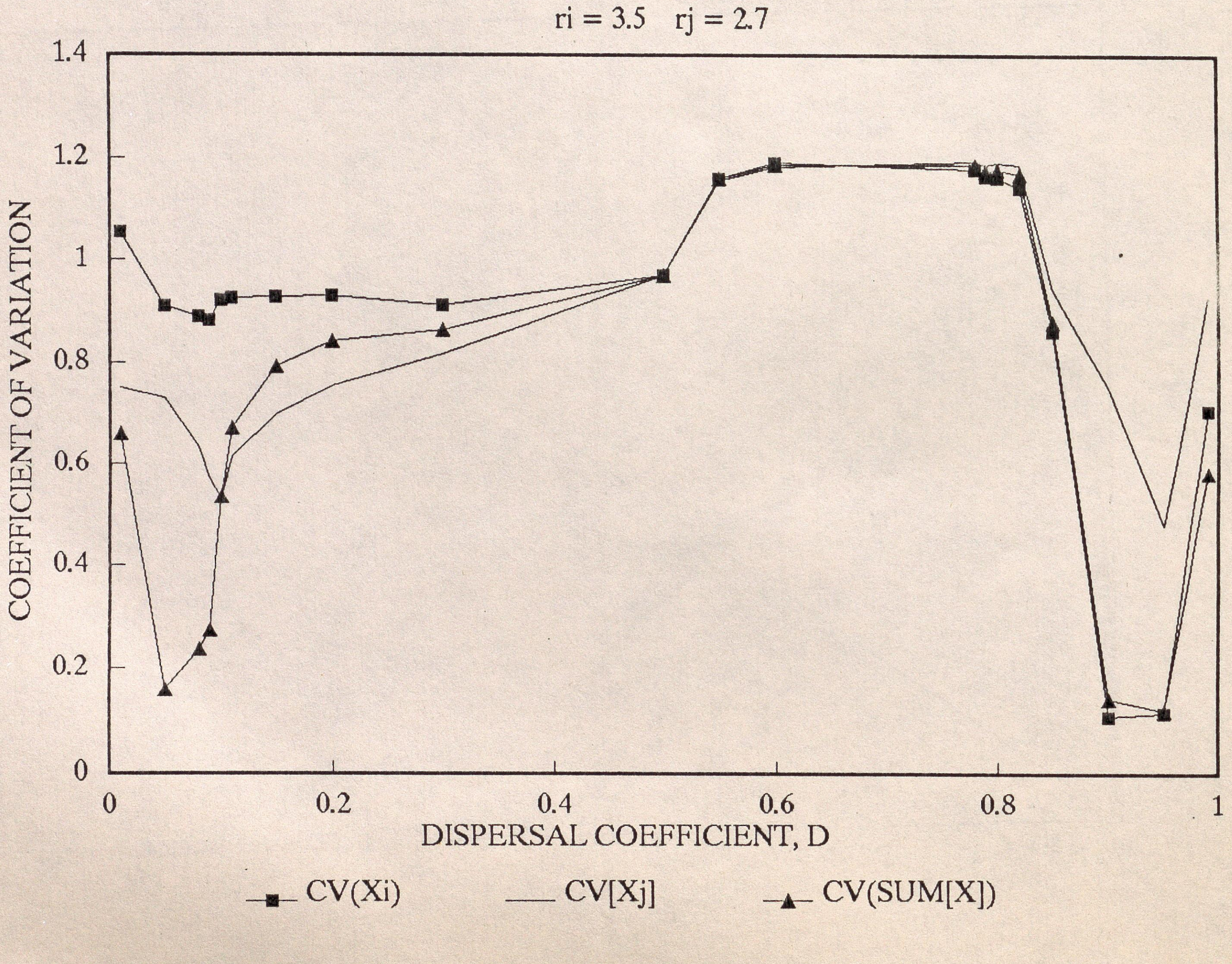

ri = 3.5 rj = 2.7
COEFFICIENT OF VARIATION
1.4
1.2
1
0.8
0.6
0.4
0.2
0
0
0.2
0.4
0.6
0.8
1
DISPERSAL COEFFICIENT, D
CV(Xi)
CV[Xj]
CV(SUM[X])

Fig 5.1.17

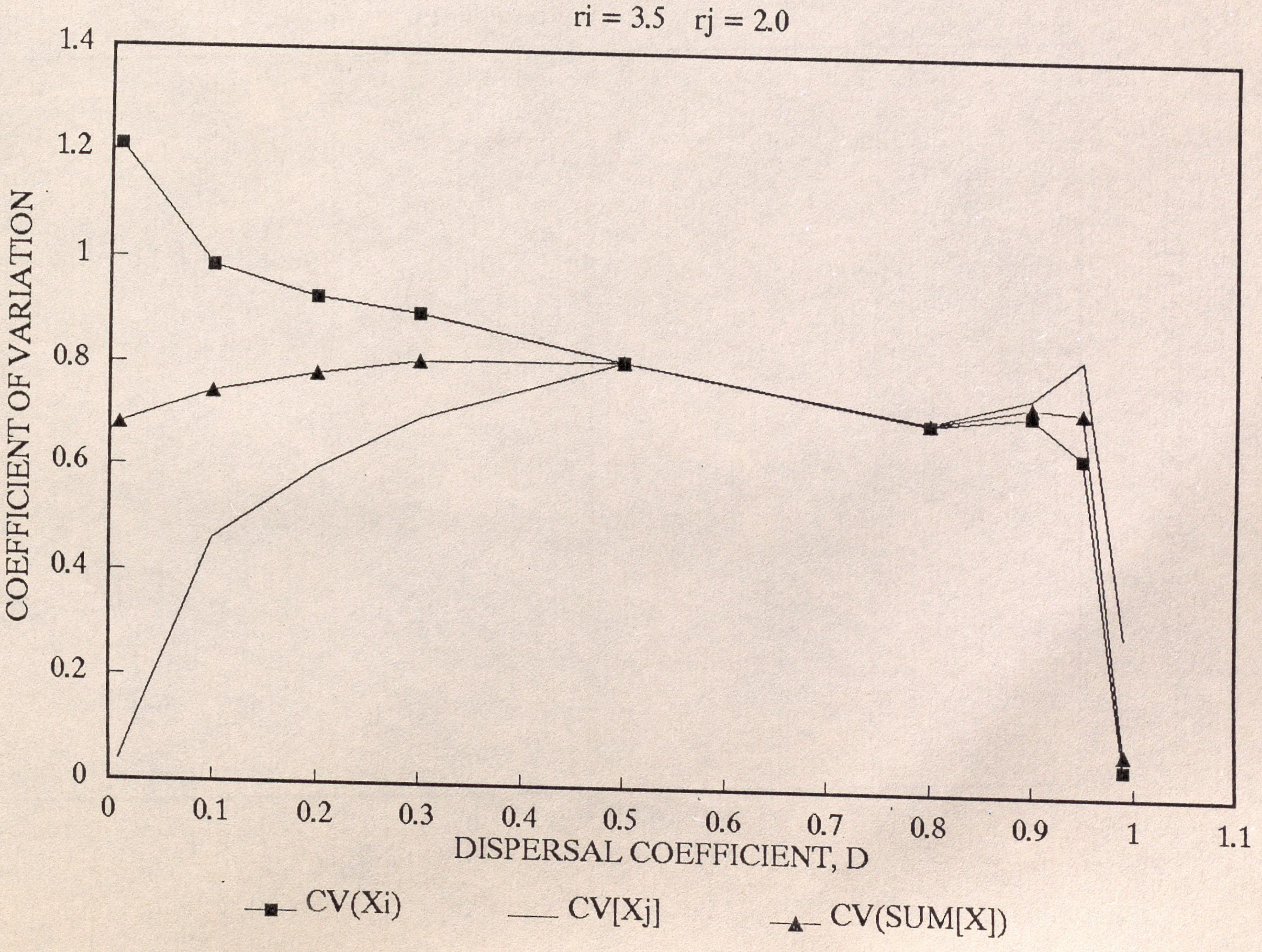

ri = 3.5 rj = 2.0
1.4
1.2
1
0.8
0.6
0.4
0.2
0
COEFFICIENT OF VARIATION
0 0.1 0.2 0.3 0.4 0.5 0.6 0.7 0.8 0.9 1 1.1
DISPERSAL COEFFICIENT, D
CV(Xi)
CV[Xj]
CV(SUM[X])

Fig 3.1.19

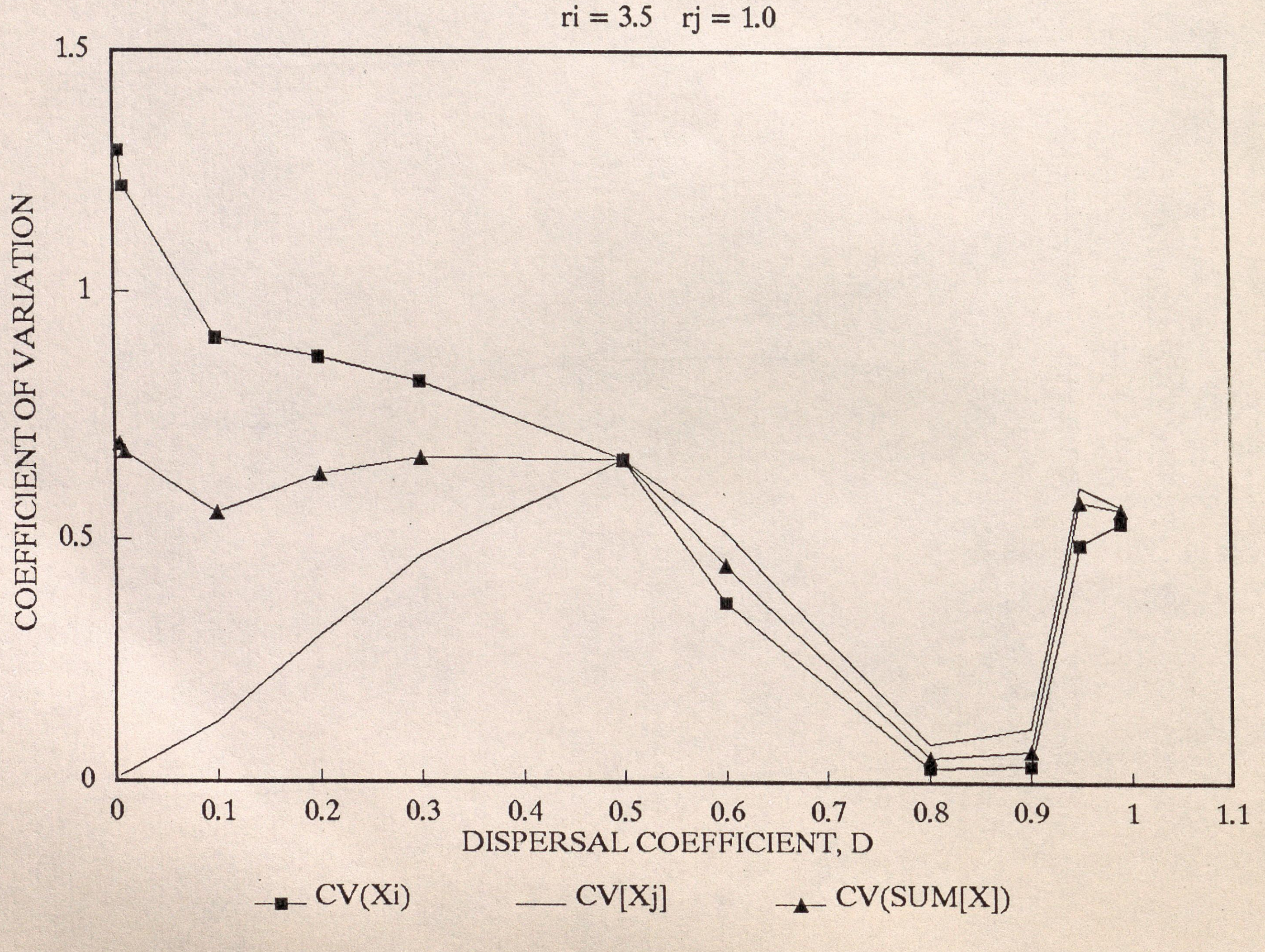
ri = 3.5 rj = 1.0
COEFFICIENT OF VARIATION
1.5
1
0.5
0
0
0.1
0.2
0.3
0.4
0.5
0.6
0.7
0.8
0.9
1
1.1
DISPERSAL COEFFICIENT, D
CV(Xi)
CV[Xj]
CV(SUM[X])

D. 1. 21

Ki = 1.0   Kj = 2.0

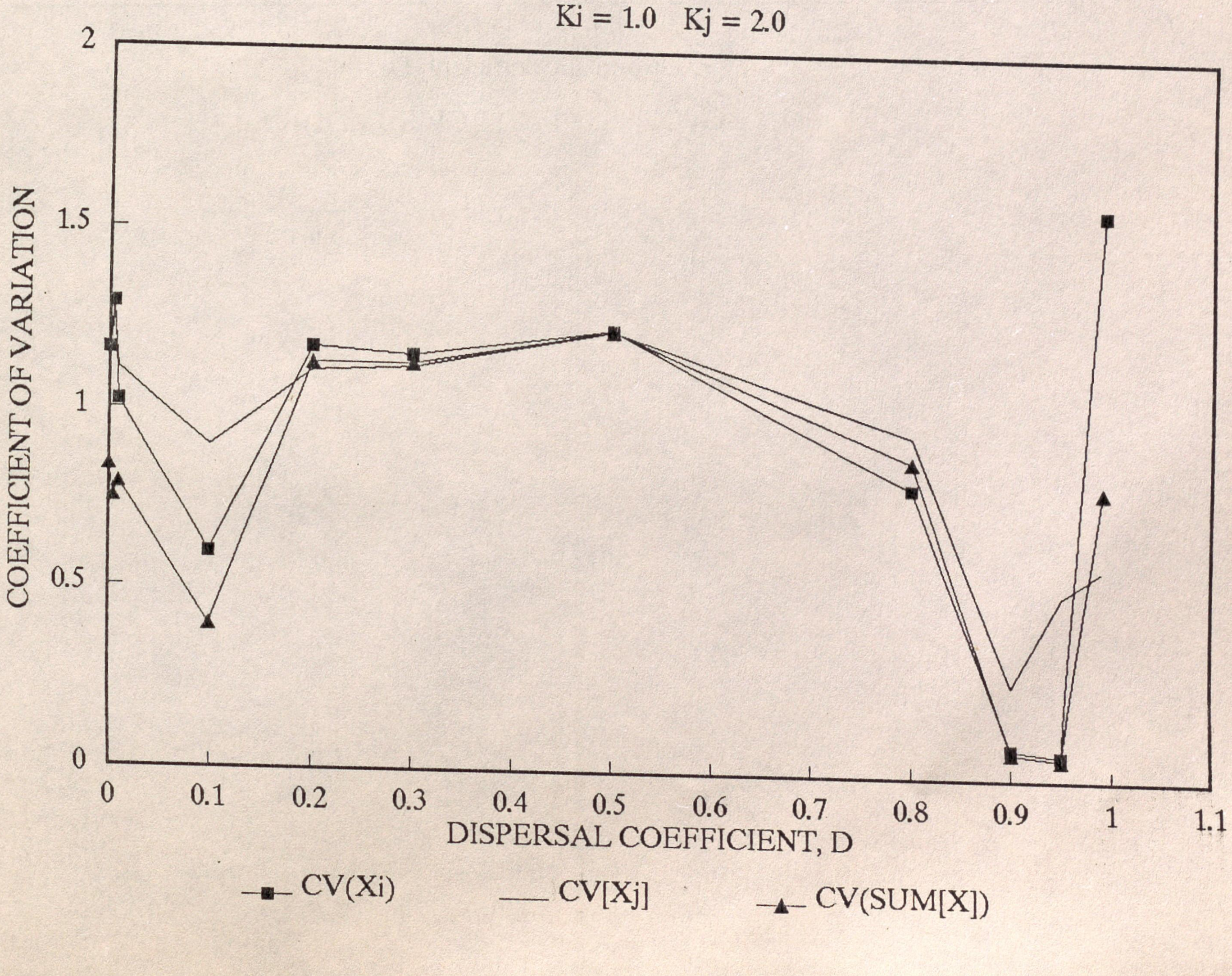

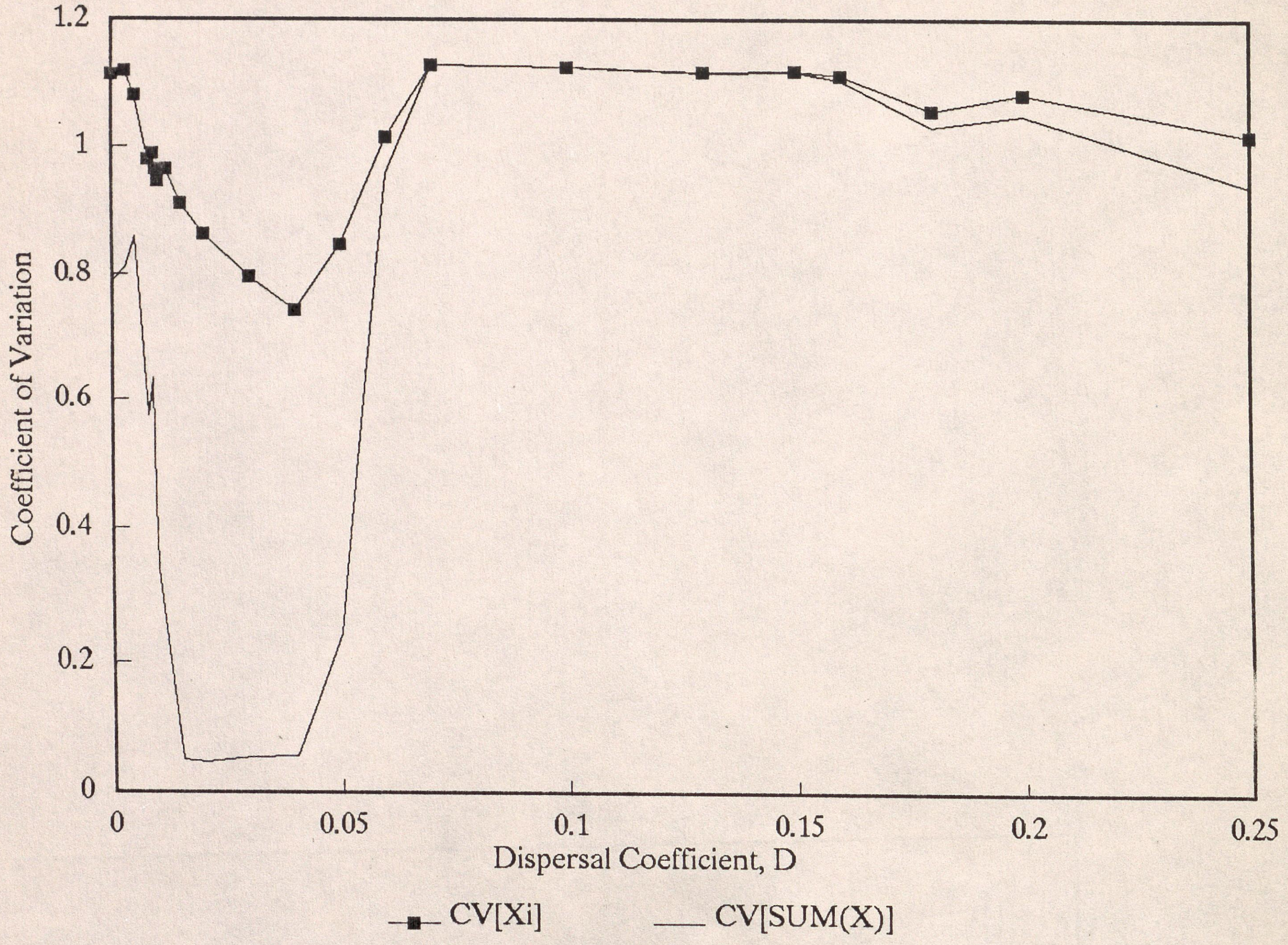
1.2
1
0.8
0.6
0.4
0.2
0
Coefficient of Variation
0
0.05
0.1
0.15
0.2
0.25
Dispersal Coefficient, D
CV[Xi]
CV[SUM(X)]

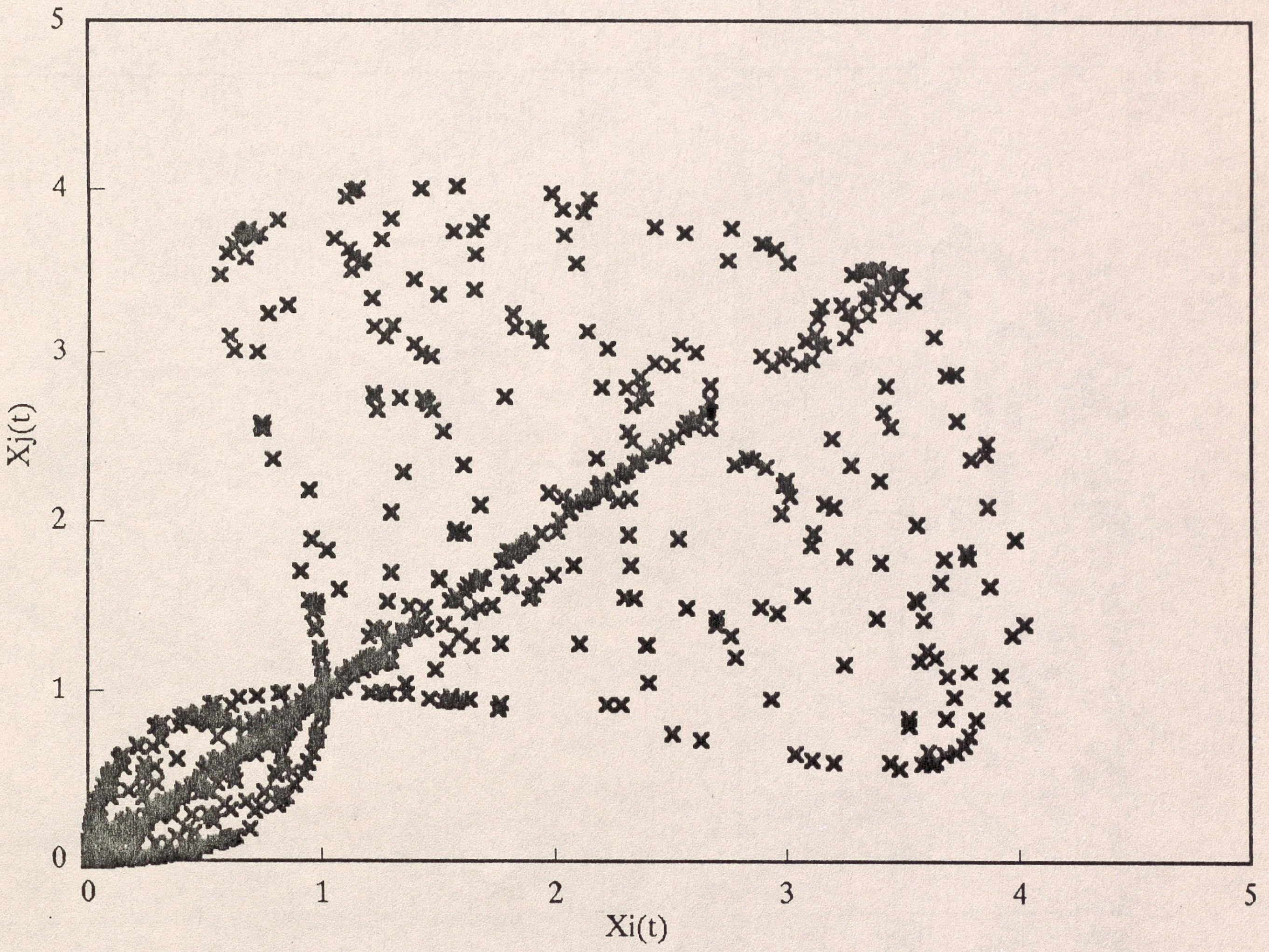

Fig. 3.2.2

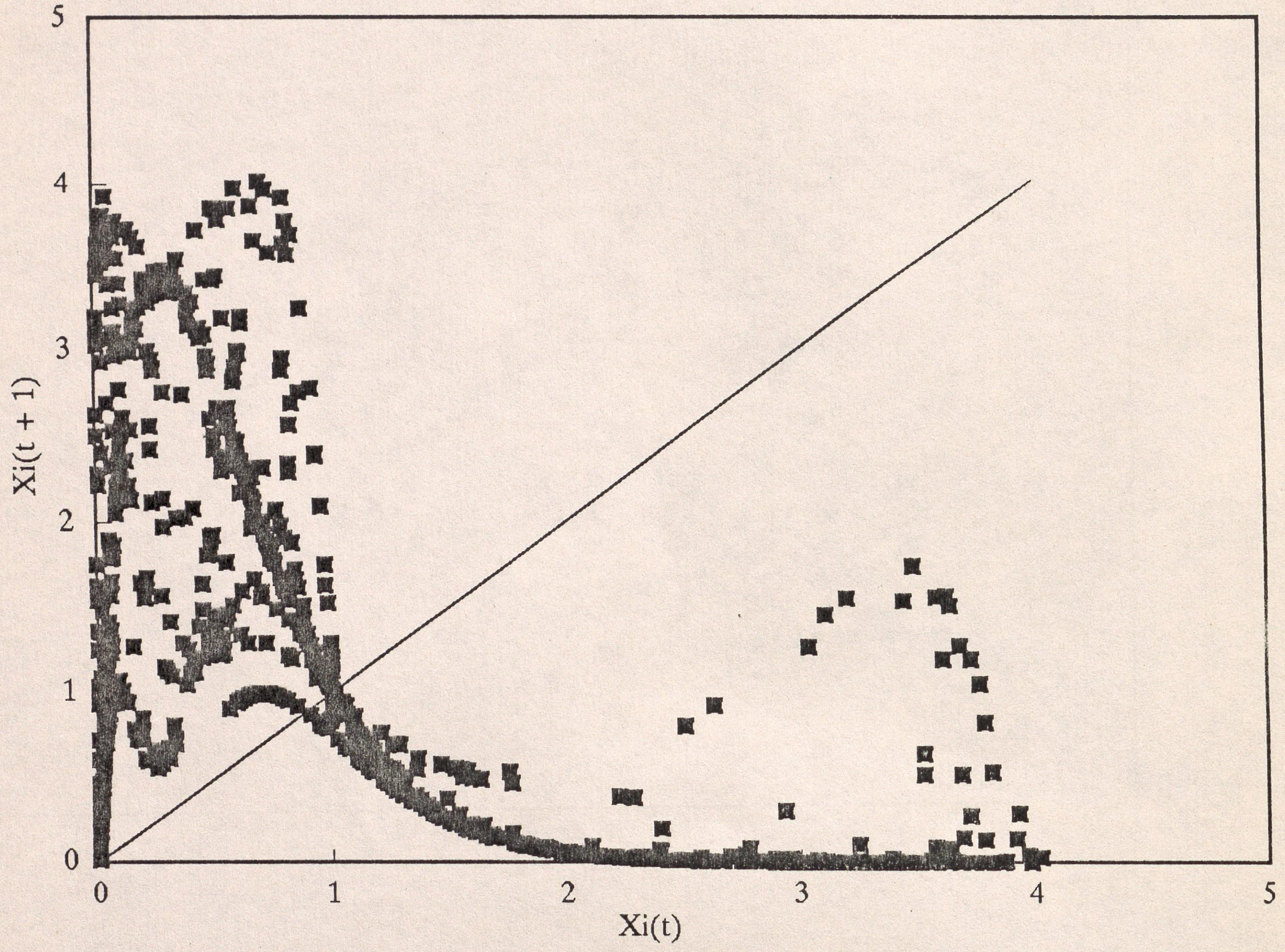

3.2.3

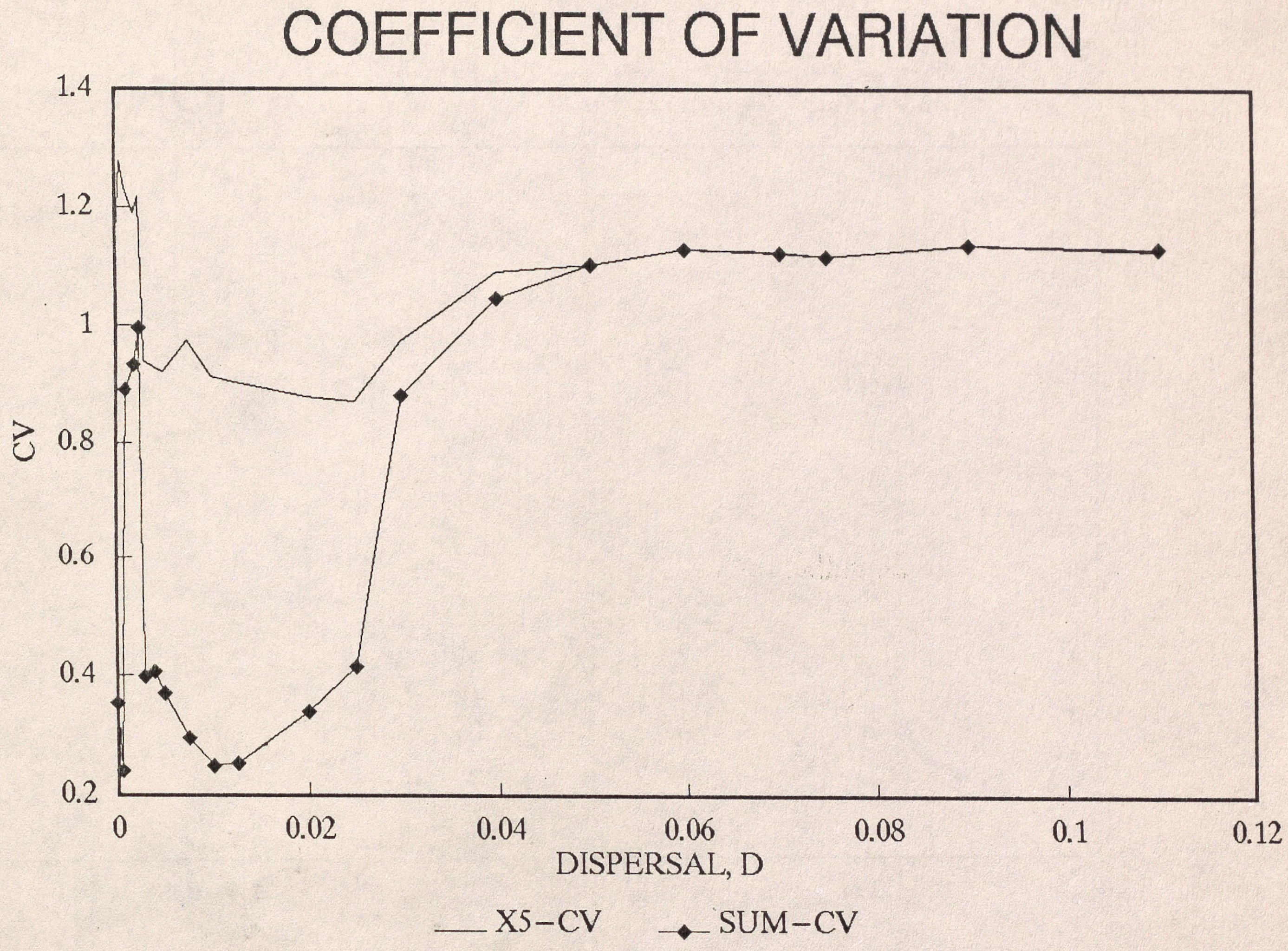
COEFFICIENT OF VARIATION
1.4
1.2
1
0.8
0.6
0.4
0.2
CV
0
0.02
0.04
0.06
0.08
0.1
0.12
DISPERSAL, D
X5-CV
SUM-CV

Fig. 4.1

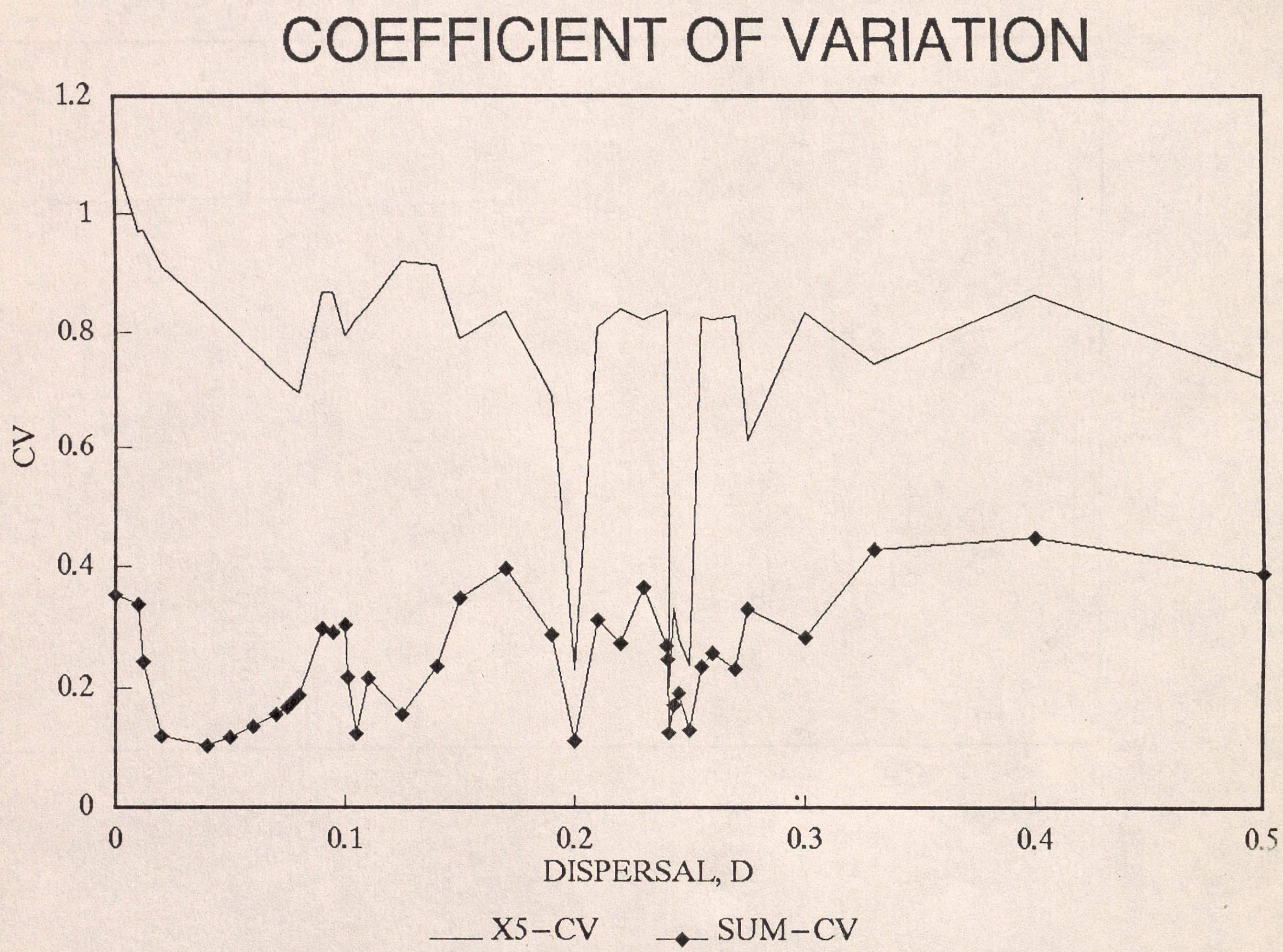
COEFFICIENT OF VARIATION
CV
DISPERSAL, D
X5-CV
SUM-CV
1.2
1
0.8
0.6
0.4
0.2
0
0
0.1
0.2
0.3
0.4
0.5

Fig. 4.2

COEFFICIENT OF VARIATION

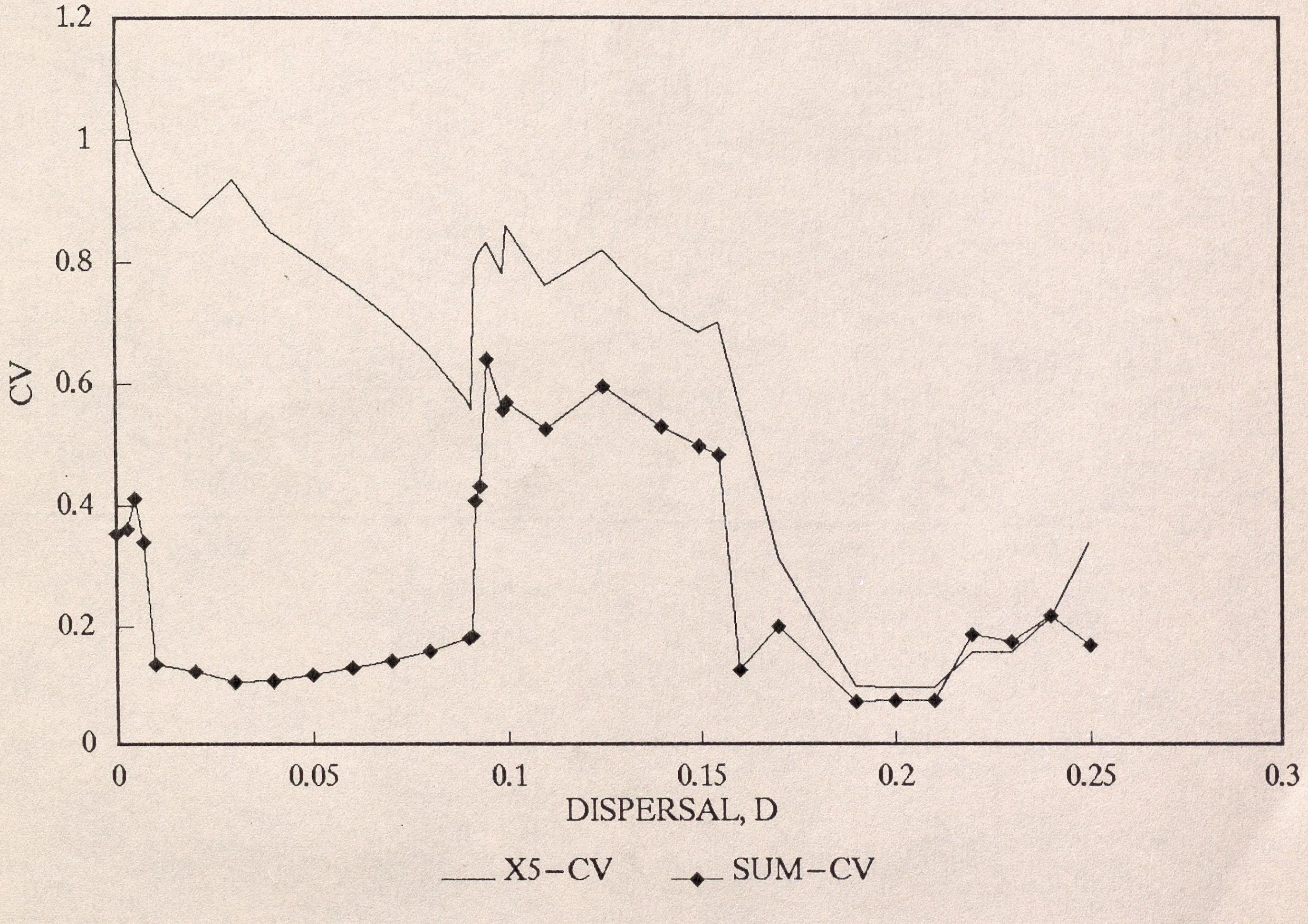

4.3

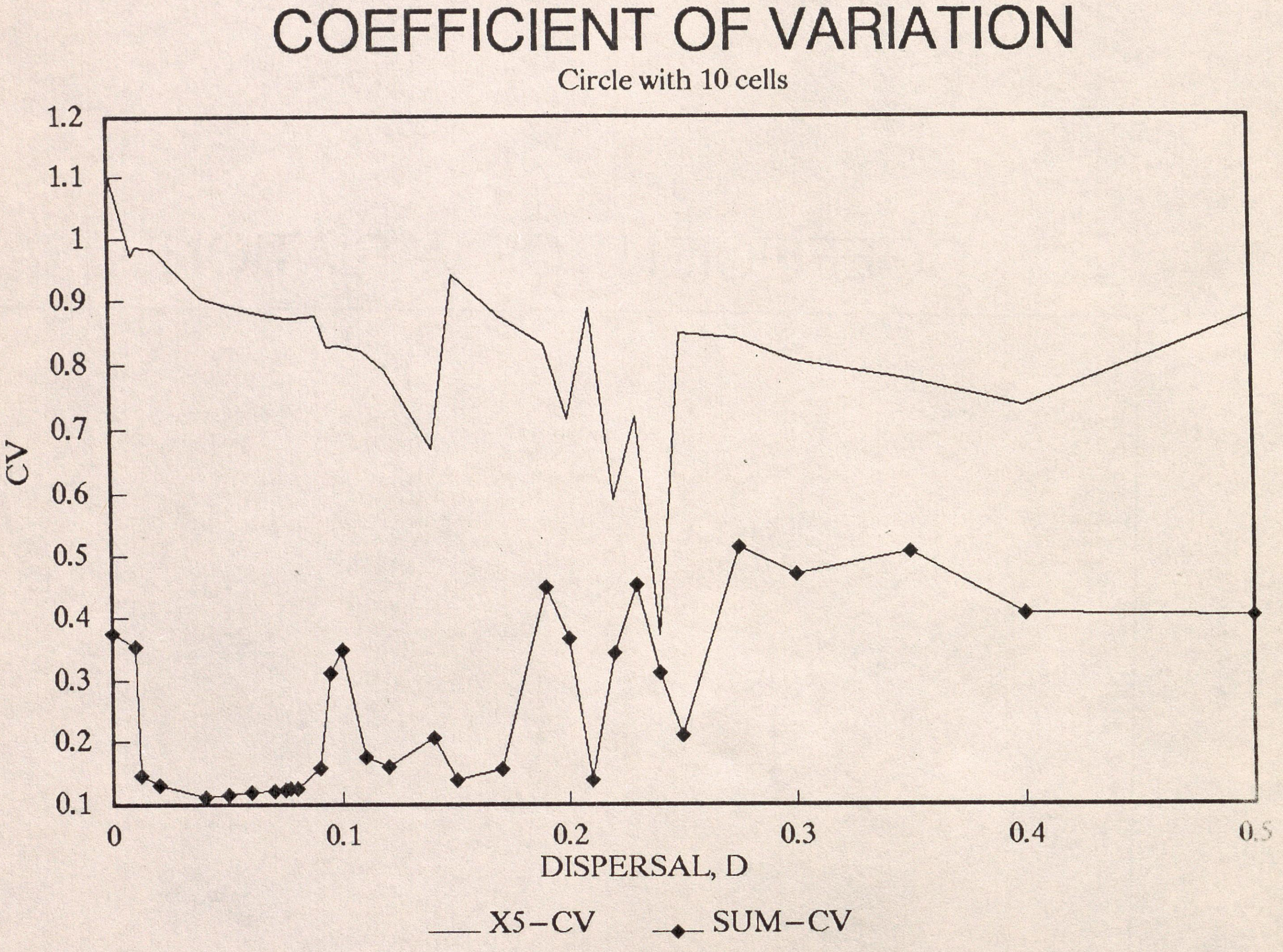
COEFFICIENT OF VARIATION
Circle with 10 cells
CV
1.2
1.1
1
0.9
0.8
0.7
0.6
0.5
0.4
0.3
0.2
0.1
0
0.1
0.2
0.3
0.4
0.5
DISPERSAL, D
X5-CV
SUM-CV

Fig. 5.1

NONLINEAR FORECASTING

RICKER MODEL WITH DISPERSAL=0.02, r=3.5

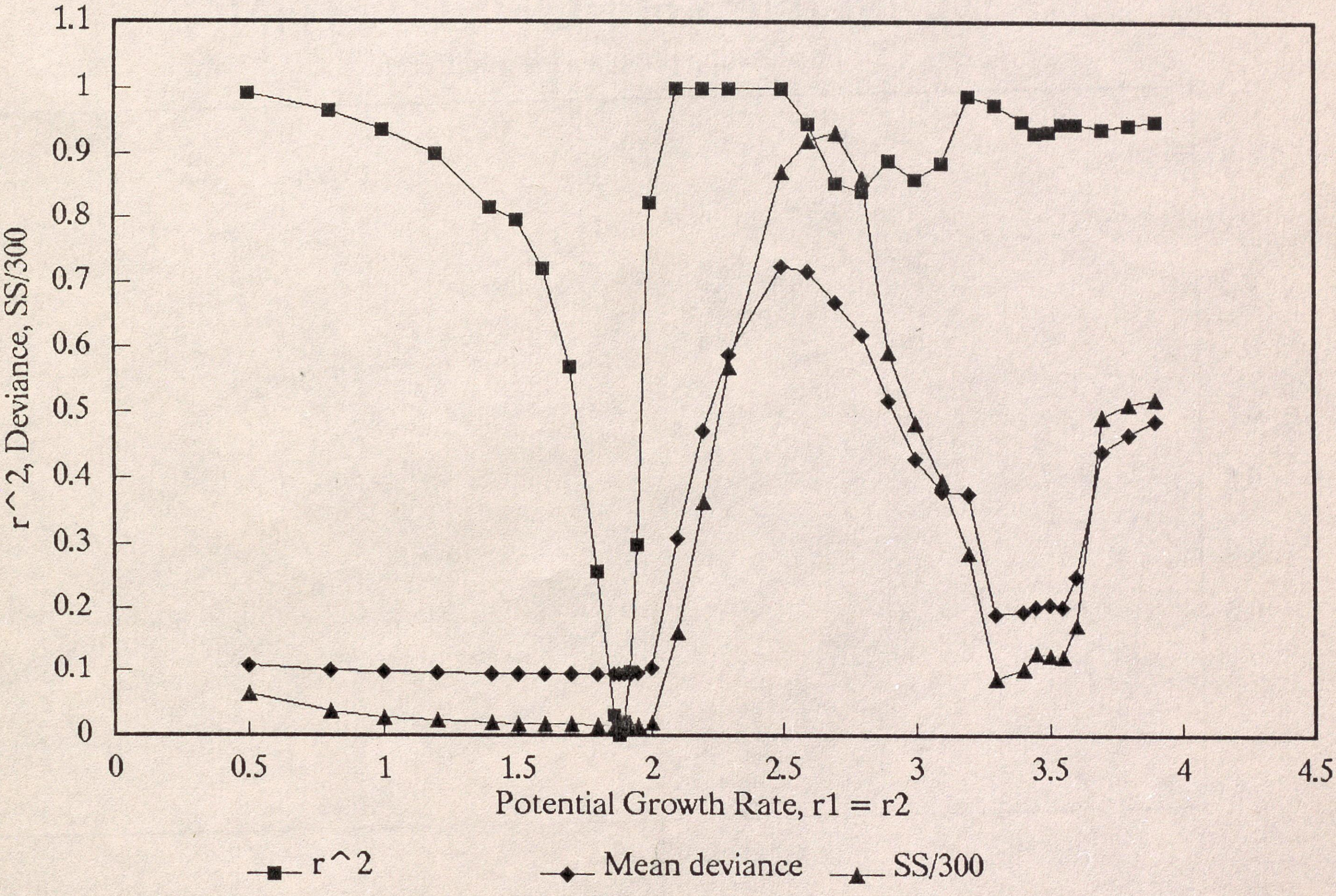

Fig. 6.2.1

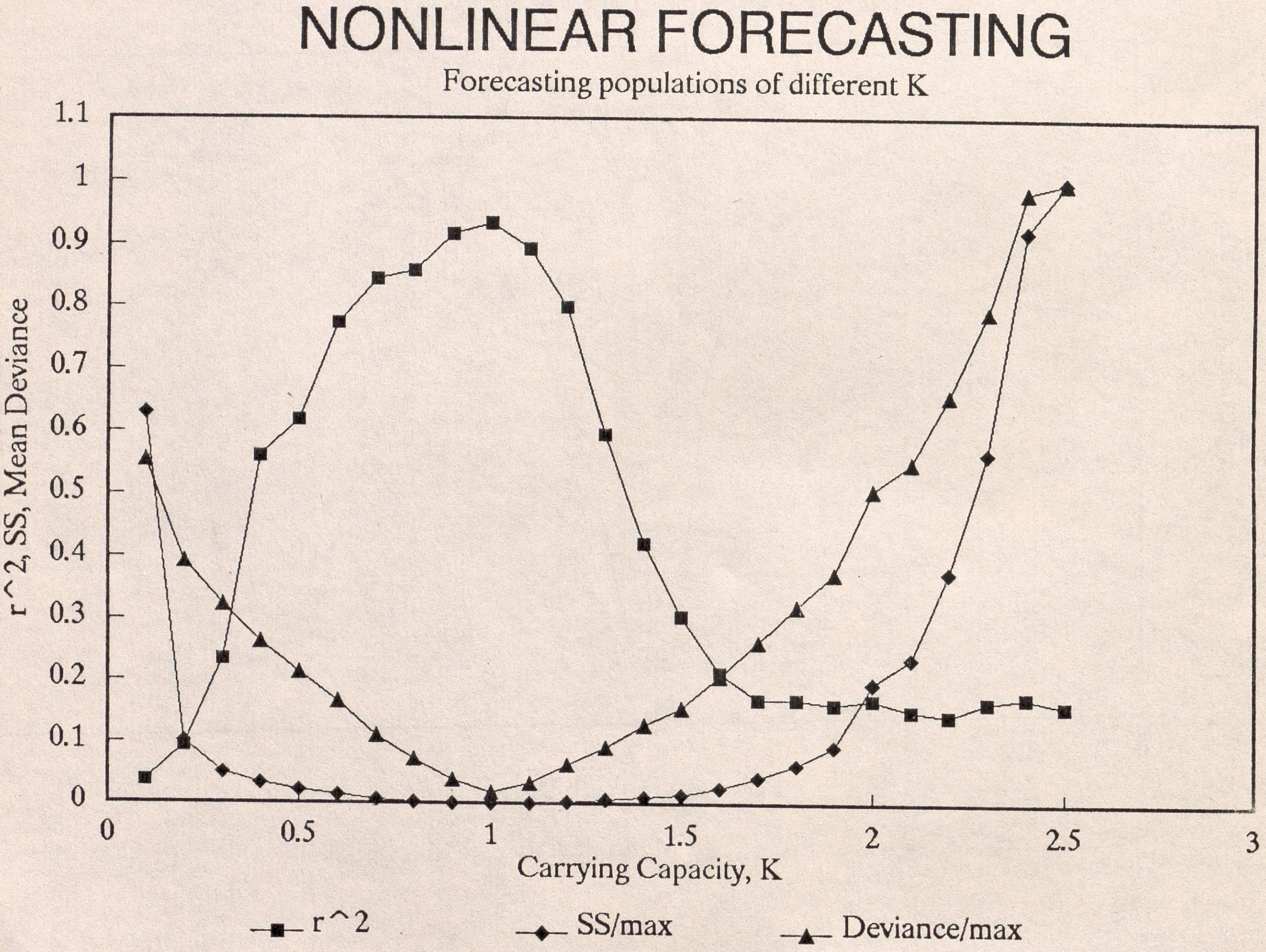
NONLINEAR FORECASTING
Forecasting populations of different K
1.1
1
0.9
0.8
0.7
0.6
0.5
0.4
0.3
0.2
0.1
0
r^2, SS, Mean Deviance
0
0.5
1
1.5
2
2.5
3
Carrying Capacity, K
r^2
SS/max
Deviance/max

6.2.2

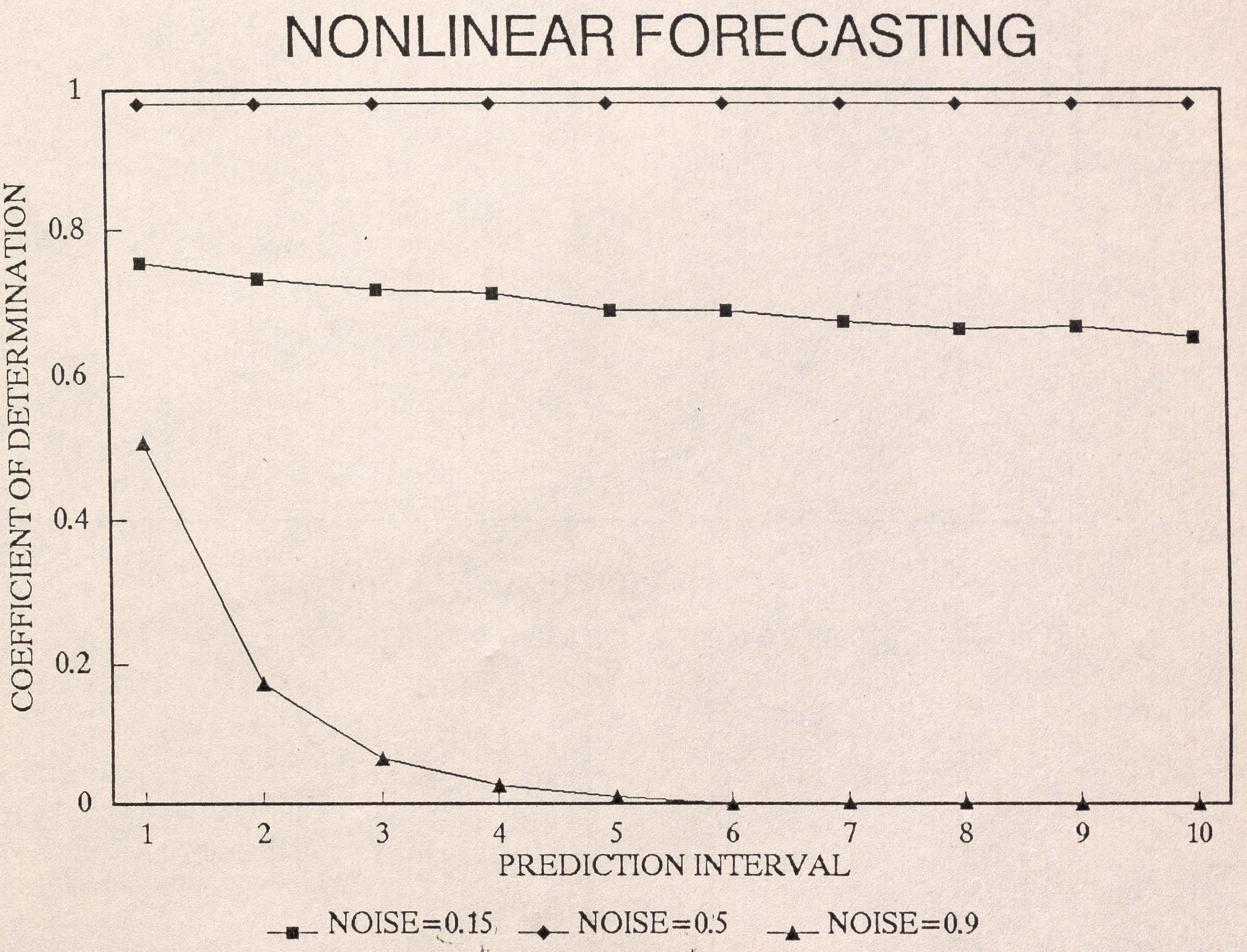
NONLINEAR FORECASTING
1
0.8
0.6
0.4
0.2
0
COEFFICIENT OF DETERMINATION
1
2
3
4
5
6
7
8
9
10
PREDICTION INTERVAL
NOISE=0.15
NOISE=0.5
NOISE=0.9

6.3.1

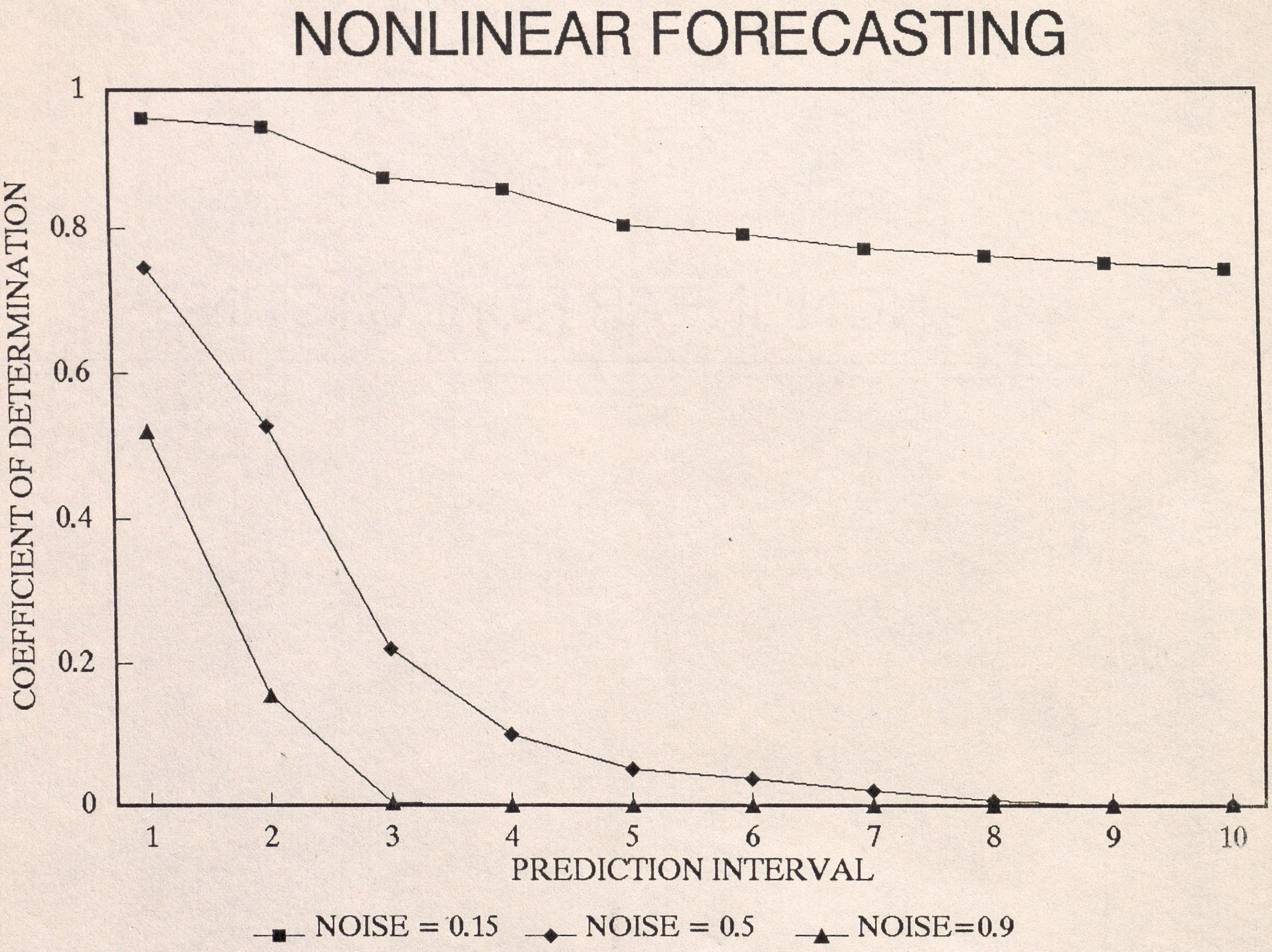
NONLINEAR FORECASTING
COEFFICIENT OF DETERMINATION
1
0.8
0.6
0.4
0.2
0
1
2
3
4
5
6
7
8
9
10
PREDICTION INTERVAL
NOISE = 0.15
NOISE = 0.5
NOISE=0.9

6.32

NONLINEAR FORECASTING

RICKER MODEL WITH DISPERSAL=0.02, r=3.5

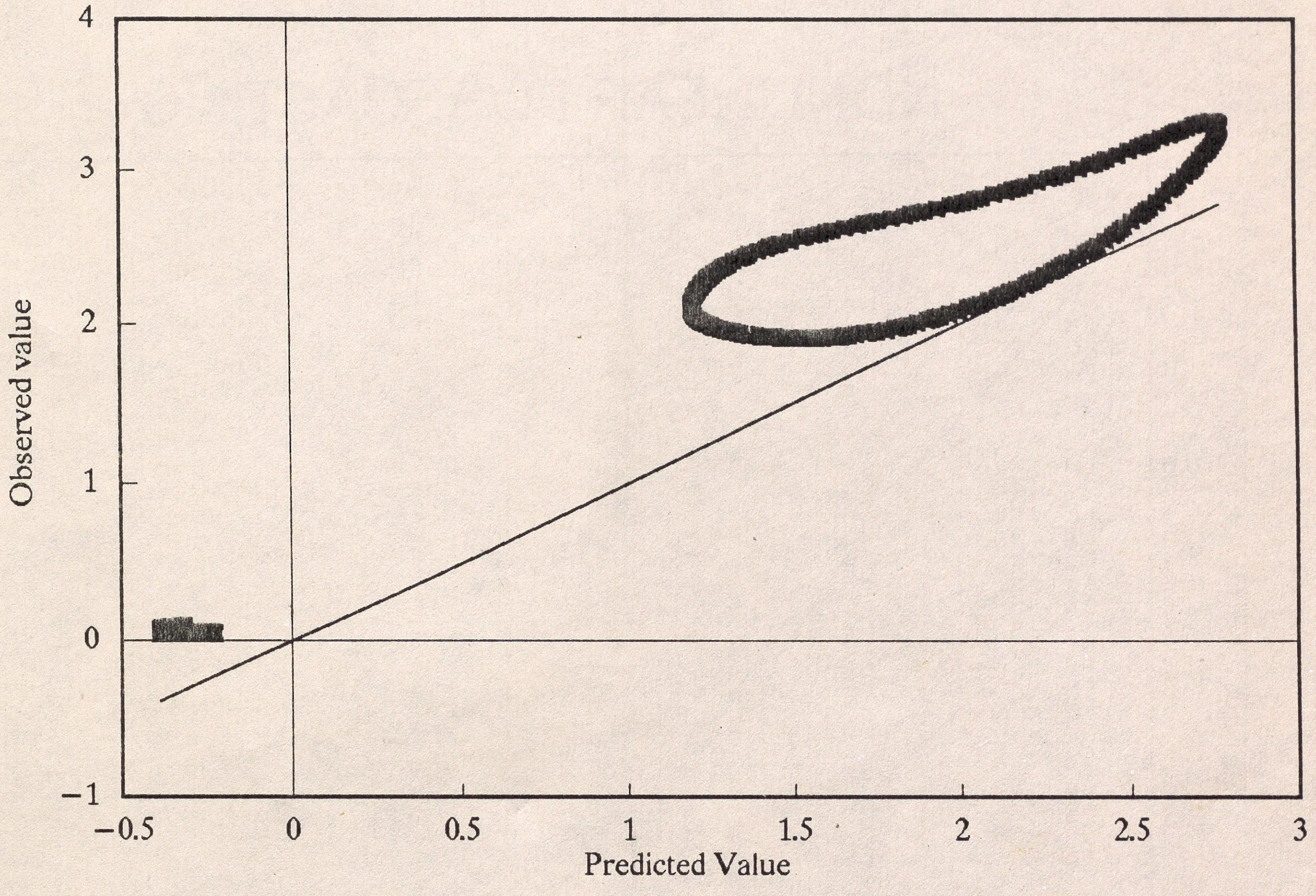

Fig 6.5.2

NONLINEAR FORECASTING

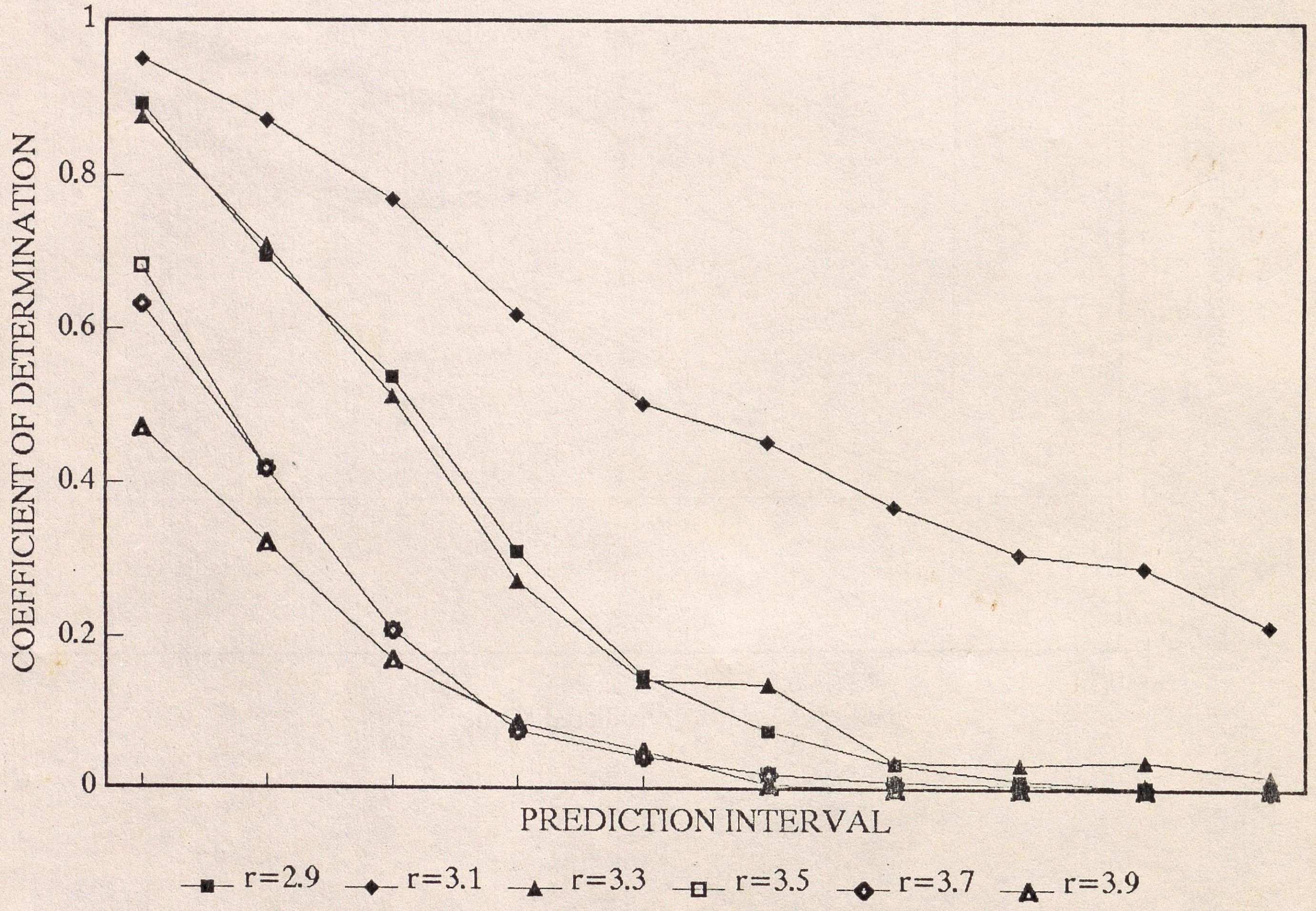

C.C.1